

World Journal of *Radiology*

World J Radiol 2023 March 28; 15(3): 56-88



REVIEW

- 56 Hepatocellular carcinoma: State of the art diagnostic imaging
Criss C, Nagar AM, Makary MS

MINIREVIEWS

- 69 Multi-modality parathyroid imaging: A shifting paradigm
Gulati S, Chumber S, Puri G, Spalkit S, Damle NA, Das CJ

CASE REPORT

- 83 Magnetic resonance imaging findings of spontaneous pyomyoma in a premenopausal woman managed with myomectomy: A case report
Martínez D, Sanchez GE, Gómez J, Sonda LJ, Suárez LD, López CS, Vega JJ, Cepeda DA

ABOUT COVER

Editorial Board Member of *World Journal of Radiology*, Wing-Chi E Kwok, PhD, Associate Professor, Department of Imaging Sciences, University of Rochester, Rochester, NY 14642, United States.
edmund_kwok@urmc.rochester.edu

AIMS AND SCOPE

The primary aim of *World Journal of Radiology (WJR, World J Radiol)* is to provide scholars and readers from various fields of radiology with a platform to publish high-quality basic and clinical research articles and communicate their research findings online.

WJR mainly publishes articles reporting research results and findings obtained in the field of radiology and covering a wide range of topics including state of the art information on cardiopulmonary imaging, gastrointestinal imaging, genitourinary imaging, musculoskeletal imaging, neuroradiology/head and neck imaging, nuclear medicine and molecular imaging, pediatric imaging, vascular and interventional radiology, and women's imaging.

INDEXING/ABSTRACTING

The *WJR* is now abstracted and indexed in PubMed, PubMed Central, Emerging Sources Citation Index (Web of Science), Reference Citation Analysis, China National Knowledge Infrastructure, China Science and Technology Journal Database, and Superstar Journals Database. The 2022 edition of Journal Citation Reports® cites the 2021 Journal Citation Indicator (JCI) for *WJR* as 0.48.

RESPONSIBLE EDITORS FOR THIS ISSUE

Production Editor: Xiang-Di Zhang; Production Department Director: Xu Guo; Editorial Office Director: Jia-Ru Fan.

NAME OF JOURNAL

World Journal of Radiology

ISSN

ISSN 1949-8470 (online)

LAUNCH DATE

January 31, 2009

FREQUENCY

Monthly

EDITORS-IN-CHIEF

Thomas J Vogl

EDITORIAL BOARD MEMBERS

<https://www.wjgnet.com/1949-8470/editorialboard.htm>

PUBLICATION DATE

March 28, 2023

COPYRIGHT

© 2023 Baishideng Publishing Group Inc

INSTRUCTIONS TO AUTHORS

<https://www.wjgnet.com/bpg/gerinfo/204>

GUIDELINES FOR ETHICS DOCUMENTS

<https://www.wjgnet.com/bpg/GerInfo/287>

GUIDELINES FOR NON-NATIVE SPEAKERS OF ENGLISH

<https://www.wjgnet.com/bpg/gerinfo/240>

PUBLICATION ETHICS

<https://www.wjgnet.com/bpg/GerInfo/288>

PUBLICATION MISCONDUCT

<https://www.wjgnet.com/bpg/gerinfo/208>

ARTICLE PROCESSING CHARGE

<https://www.wjgnet.com/bpg/gerinfo/242>

STEPS FOR SUBMITTING MANUSCRIPTS

<https://www.wjgnet.com/bpg/GerInfo/239>

ONLINE SUBMISSION

<https://www.f6publishing.com>

Hepatocellular carcinoma: State of the art diagnostic imaging

Cody Criss, Arpit M Nagar, Mina S Makary

Specialty type: Radiology, nuclear medicine and medical imaging

Provenance and peer review: Invited article; Externally peer reviewed.

Peer-review model: Single blind

Peer-review report's scientific quality classification

Grade A (Excellent): A
Grade B (Very good): B
Grade C (Good): 0
Grade D (Fair): 0
Grade E (Poor): 0

P-Reviewer: Kumar SKY, India;
Papadopoulos N, Greece

Received: December 18, 2022

Peer-review started: December 18, 2022

First decision: January 31, 2023

Revised: February 12, 2023

Accepted: March 22, 2023

Article in press: March 22, 2023

Published online: March 28, 2023



Cody Criss, Heritage College of Osteopathic Medicine, Ohio University, Athens, OH 45701, United States

Arpit M Nagar, Mina S Makary, Department of Radiology, The Ohio State University Medical Center, Columbus, OH 43210, United States

Corresponding author: Mina S Makary, MD, Assistant Professor, Attending Doctor, Director, Department of Radiology, The Ohio State University Medical Center, 395 W. 12th Ave., Columbus, OH 43210, United States. mina.makary@osumc.edu

Abstract

Primary liver cancer is the fourth most common malignancy worldwide, with hepatocellular carcinoma (HCC) comprising up to 90% of cases. Imaging is a staple for surveillance and diagnostic criteria for HCC in current guidelines. Because early diagnosis can impact treatment approaches, utilizing new imaging methods and protocols to aid in differentiation and tumor grading provides a unique opportunity to drastically impact patient prognosis. Within this review manuscript, we provide an overview of imaging modalities used to screen and evaluate HCC. We also briefly discuss emerging uses of new imaging techniques that offer the potential for improving current paradigms for HCC characterization, management, and treatment monitoring.

Key Words: Hepatocellular carcinoma; Imaging; Diagnostic; Magnetic resonance imaging; Computed tomography; Ultrasound; Radiogenomics

©The Author(s) 2023. Published by Baishideng Publishing Group Inc. All rights reserved.

Core Tip: Successful tumor assessment can be a critical component to patient management and prognosis. The expansion of imaging techniques beyond conventional modalities (e.g. ultrasound, computed tomography, magnetic resonance imaging) provides an opportunity to improve the identification of small or well-differentiated hepatocellular carcinoma tumors, along with the capability to monitor treatment responses to surgery or locoregional therapy.

Citation: Criss C, Nagar AM, Makary MS. Hepatocellular carcinoma: State of the art diagnostic imaging. *World J Radiol* 2023; 15(3): 56-68

URL: <https://www.wjgnet.com/1949-8470/full/v15/i3/56.htm>

DOI: <https://dx.doi.org/10.4329/wjr.v15.i3.56>

INTRODUCTION

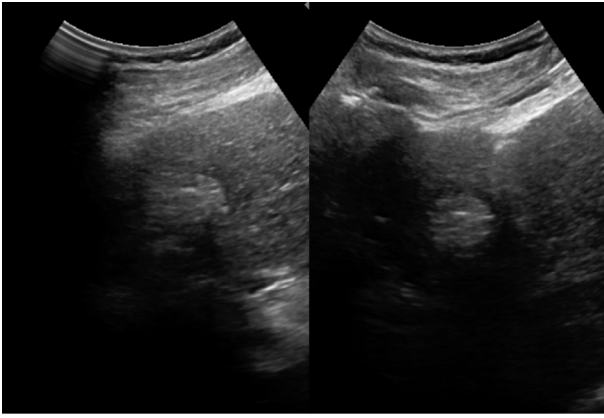
Hepatocellular carcinoma (HCC) is the most common liver malignancy, accounting for 90% of liver tumors, and a leading cause of mortality worldwide[1,2]. Global risk factors for HCC include cirrhosis, existing in up to 90% of new cases[3], or patients with long-standing liver infections such as viral hepatitis B and C[4]. East Asia and sub-Saharan Africa account for greater than 80% of cases, and incidence within the United States continues to rise[3,4]. Unfortunately, many patients are diagnosed in the advanced stages of the disease, which emphasizes the importance of early detection and surveillance [5]. Surveillance and early tumor detection using ultrasonography is recommended by the American Association for the Study of Liver Diseases (AASLD) for high-risk populations driven by ultrasound-guided imaging. Unlike other malignancies, HCC expresses distinctive characteristics that can be diagnosed based on imaging features alone, without the need for confirmation from tissue sampling[6]. In this review, we provide a summary of diagnostic criteria and imaging modalities used to detect and stage HCC, as well as emerging methods to further assist in the surveillance and characterization of the disease.

SURVEILLANCE AND SCREENING

Conventional ultrasound

Tumor burden can significantly impact management, where patients with small, localized tumors can receive curative methods such as liver transplantation, resection, or locoregional therapies. On the other hand, treatment options are limited in patients with HCC displaying more aggressive features (*e.g.*, extrahepatic metastases, multifocal tumors, and vascular invasion). As a result, early detection may offer a significant benefit in select patients. Patient populations recommended for HCC surveillance differs between AASLD[7], the European Association for the Study of the Liver (EASL)[8] and the Asian Pacific Association for the Study of the Liver (APASL)[9], but largely consist of adults with cirrhosis or patients with hepatitis B virus (HBV)[10]. Across surveillance recommendations, biannual abdominal ultrasonography (Figure 1) is the standard modality for HCC detection with major advantages including accessibility, cost-effectiveness, and safety[10].

Surveillance programs typically consist of ultrasound examination performed at either 6- or 12-mo intervals. Across all stages of HCC, ultrasound detection carries 84% sensitivity. A number of investigations have found a mortality and cost-benefit of biannual ultrasonography for imaging surveillance of HCC[10-12]. For example, a study in HBV-infected patients in China found a 37% reduction in mortality in those receiving biannual ultrasonography examinations compared to the control group[12]. Suboptimal visualization poses a major limitation for ultrasound screening. Poor visualization and sonographic sensitivity to HCC lesions can be caused by a number of different extrinsic factors such as morbid obesity, patient inability to suspend respiration, obscured portions of the liver by bowel gas or rib shadowing, and intrinsic factors such as hepatic steatosis or fibrosis causing parenchymal heterogeneity[13]. A recent investigation reported approximately 20% of scans were inadequate to exclude liver lesions[14]. Detecting smaller nodules (< 2 cm) appears to be a major limitation of ultrasound, with studies reporting detection rates as low as approximately 28%[15]. In response, the American College of Radiology (ACR) screening guidelines have recommended the use of systematic documentation and scoring for visualization (A: No or minimal limitations; B: Moderate limitations; C: Severe limitations). The use of tumor biomarkers, such as alpha-fetoprotein (AFP), in concert with ultrasound examination appears to have an additive effect on detection rate[16]. For example, a recent meta-analysis of prospective studies found the sensitivity for ultrasound alone to detect any stage of HCC was 78% compared to 97% when adding AFP[17]. Interestingly, the synergistic impact of combining ultrasound with AFP also exists for detection of earlier, smaller nodules (45% *vs* 63% sensitivity, respectively)[17] which is particularly salient given the limitations of ultrasound and earlier stages of HCC. This is not without controversy, however. The 2018 AASLD guidelines do not designate any preferences between adjunctive use of AFP while the 2017 APASL guidelines recommend the combination of ultrasound and AFP[18]. In contrast, the 2018 EASL guidelines discourage the use of ultrasound with AFP for 6-mo HCC surveillance, citing concerns of false-positives in the setting of active liver inflammation with infection[18].



DOI: 10.4329/wjr.v15.i3.56 Copyright ©The Author(s) 2023.

Figure 1 Screening ultrasound. Hyperechoic segment IV liver lesion compatible and later characterized as hepatocellular carcinoma.

While the objective of this review is to elucidate the latest advancements in technological imaging for the screening and diagnosis of HCC, it is important to note the efficacy of detection can be limited due to multifactorial screening challenges. In fact, less than 1 in 5 patients with cirrhosis receive surveillance screening for HCC[19]. Previous reviews have extensively examined the numerous challenges encountered during the screening process, including the inability to properly stratify high-risk patients, the presence of socio-economic and logistical impediments to accessing healthcare, as well as training and detection limitations using conventional imaging techniques, as previously discussed. One of the most common attributable factors to surveillance underuse includes lack of surveillance orders or unrecognized cirrhosis[5]. Therefore, strategies to improve education and integrating primary care providers in surveillance efforts can have a drastic and meaningful effect on rates of patients undergoing HCC screening[20]. The implementation of patient-centered outreach programs such as reminder protocols or embedding best-practice advisories within the electronic health record may be solutions to improve barriers of patients undergoing surveillance[5,20]. The decision to select which patients to screen also been discussed and studies have developed scoring systems across different risk factors (*e.g.* hepatitis or cirrhosis) to refine and improve risk stratification have been proposed[21]. Other methods have also focused on improving surveillance outcomes and detection rates, such as utilizing serological biomarkers (*e.g.* AFP) either as a single screening modality or in concert with imaging to improve sensitivity, at the potential cost of increased rates of false positivity. The use of biomarkers may also be especially helpful for smaller HCCs, not easily visible with ultrasound[21].

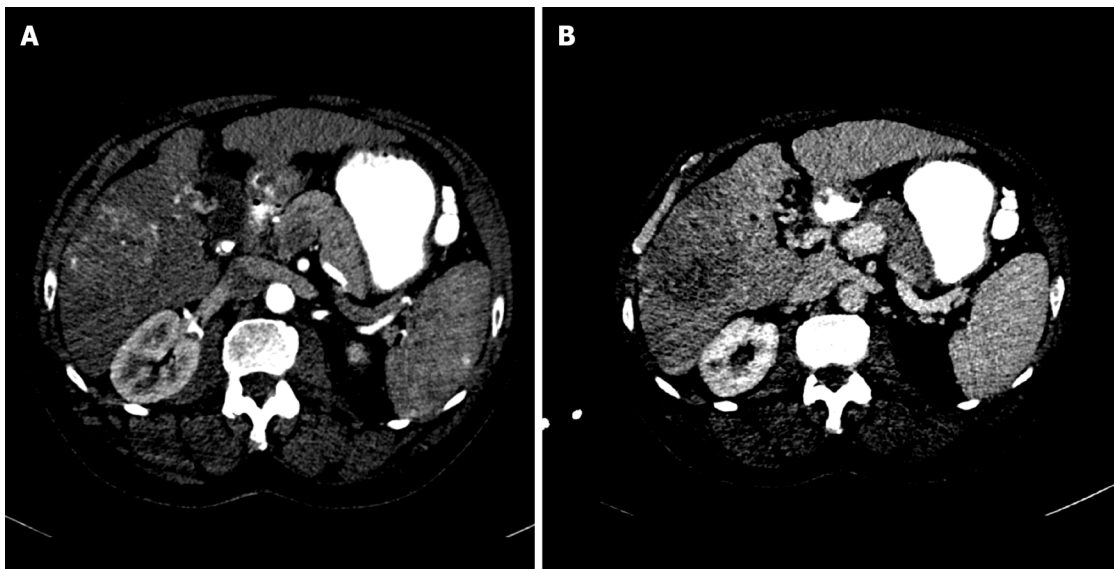
HCC DIAGNOSTIC MODALITIES

Liver imaging reporting and data systems diagnostic reporting system

Established by the ACR, standardized methods for imaging interpretation and reporting are defined using the liver imaging reporting and data systems (LI-RADS). The application of the LI-RADS diagnostic algorithm was initially developed for computed tomography (CT)/magnetic resonance imaging (MRI). LI-RADS is subdivided into 8 categories and ranges in greater probability of malignancy from LR-1 to LR-5 with additional categories including LI-RADS M (LR-M) (probably or definitely malignant but not HCC specific), LR-definite tumor in vein, and LR-cannot be categorized (NC)[13,22]. Observation of lesions categorized in LR-5 is designated as almost certainly HCC, with a systematic review of 454 studies reporting 94% of LR-5 lesions confirmed to be HCC and 97% malignant[23]. The Organ Procurement and Transplantation Network (OPTN) is another diagnostic criterion established by National Organ Transplant Act, with subcategories ranging from class 0-5. Specificities are similar between LI-RADSv2018 LR-5 and OPTN class 5[24]. However, inter-reader agreement and sensitivity of LI-RADS (sensitivity: 63.9%) is higher than that of OPTN (sensitivity: 53.6%)[24].

Cross-sectional imaging: Multiphase CT and MRI

Standard recommendations for HCC diagnosis include multiphase CT or MRI which are beneficial modalities for highlighting unique features of HCC (Figures 2 and 3). Physiological differences in blood perfusion between hepatocarcinogenic lesions and non-neoplastic tissue display distinguishing differences in imaging characteristics using multiphasic contrast examinations[25]. Phases consist of late hepatic arterial (20-40 s), portal venous (60-90 s), and delayed (3-5 min). Late arterial phase is useful for detecting hypervascular lesions with HCC lesions characteristically enhancing relative to surrounding liver parenchyma. Arterial lesion enhancement can be appreciated within lesions as small as 1 cm.



DOI: 10.4329/wjr.v15.i3.56 Copyright ©The Author(s) 2023.

Figure 2 Axial multiphase computed tomography imaging 75-year-old male with suspected hepatocellular carcinoma. A: Hyperenhancing liver lesion in segment VIII during the arterial phase; B: Corresponding washout within the delayed venous phase.



DOI: 10.4329/wjr.v15.i3.56 Copyright ©The Author(s) 2023.

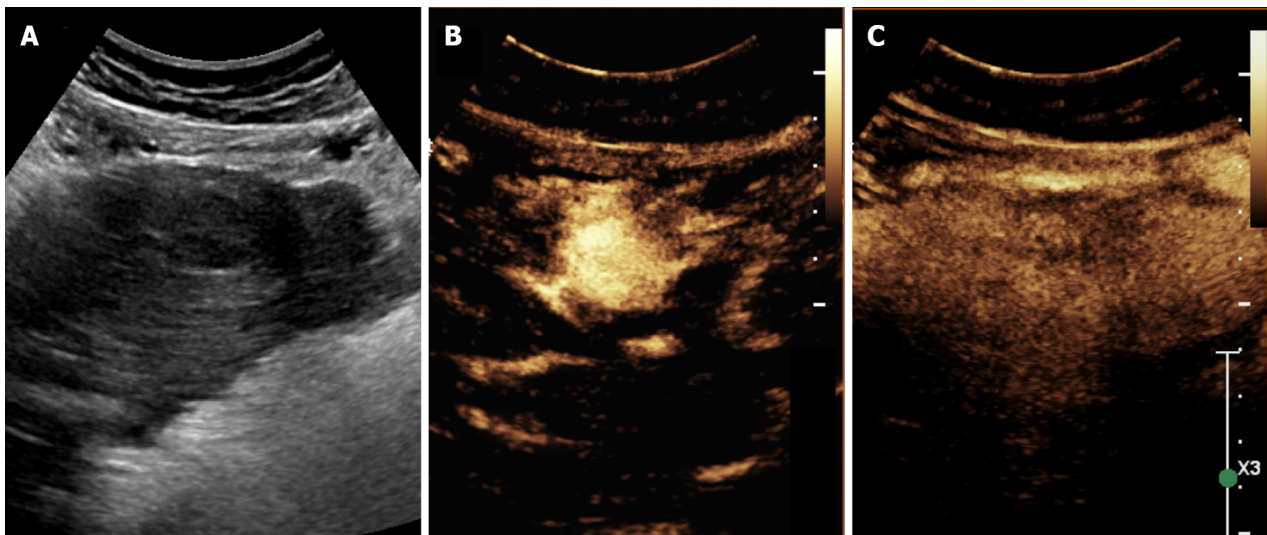
Figure 3 Axial multiphase magnetic resonance imaging. A: T2-weighted axial sequence imaging of the abdomen; B: T1-weighted fat saturation post-contrast axial sequence image of the abdomen with arterial enhancement of segment VIII lesion; C: Delayed venous phase washout.

Within the portal venous and delayed phases, washout or hypointensity is commonly observed for HCC lesions[26]. During the delayed or equilibrium phase, other characteristics of HCC such as capsule features (*e.g.* lesion washout with pseudocapsule enhancement) and mosaic architecture can be visualized[26]. The introduction of gadolinium-based contrast agents (Gadobenate dimeglumine and gadoxetate acid) may aid LI-RADS categorization. These agents are taken up by hepatocytes of normal liver parenchyma and there is little uptake in non-functioning or dysfunctional hepatocytes, such as the case for HCC. Gadolinium-based agents function similarly to extracellular agents, but can aid in the diagnosis of lesions with atypical features (*e.g.* without washout, arterial hyperenhancement) or distinguish HCC from pseudolesions[27,28]. For example, these agents permit an additional post-contrast hepatobiliary phase, which will display a majority of HCC lesions (90%-95%) as hypointense relative to surrounding hyperintense liver parenchyma[27,29].

MRI is recommended for staging of HCC disease given that some reports have estimated CT to underestimate 52% of cases[1,2]. MRI also has superior diagnostic efficiency to CT in the detection of small (≤ 3 cm) lesions[30]. However, CT is more readily available than MRI, and limitations to using MRI including greater costs and technical complexity make CT a complementary diagnostic alternative[31, 32]. A report showed that the combined use of CT/MRI provides better diagnostic accuracy in characterizing liver lesions using LI-RADS (91.29%) than MRI (85.37%) or CT (67.6%) alone, but combined protocols should be limited to difficult or uncertain cases in order to warrant use[32].

Contrast-enhanced ultrasound

In recent years, there has been an emerging use of contrast-enhanced ultrasound (CEUS) for the evaluation of focal liver lesions (Figure 4). CEUS combines the benefit of accessible, non-invasive assessment without ionizing radiation as well as improvements in temporal resolution. Given some of



DOI: 10.4329/wjr.v15.i3.56 Copyright ©The Author(s) 2023.

Figure 4 Contrast-enhanced ultrasound. A: 62-year-old female with lesion in segment III with hepatocellular carcinoma; B: Gray-scale conventional ultrasound; C: Contrast-enhanced ultrasound revealing hyperechoic lesion in arterial phase with corresponding washout in venous phase.

the limitations in ultrasound sensitivity, CEUS may offer a useful solution. CEUS utilizes highly echogenic microbubble contrast agents (such as SonoVue[®], Definity[®]) which are rapidly injected *via* the antecubital vein. These agents circulate freely among capillary beds, and the use of dynamic phases of contrast enhancement [*e.g.* arterial (start 10-20 s), portal (start 30-45 s), late (start > 120 s) phases] can help differentiate liver lesions[33].

The reporting system was initially developed for CT and MRI; however, in 2016, CEUS-LIRADS was released to improve standardization in reporting and interpretation specific to CEUS for nodule evaluation[33]. CEUS LI-RADS consists of 8 categories and ranges in greater levels of severity from LR-1 to LR-5, with additional categories such as LR-M (probably or definitely malignant but not HCC specific), LR-TIV, and LR-NC[33]. Diagnostic features of CEUS LI-RADS are based on arterial phase hyperenhancement and washout, or reductions in enhancement relative to the liver[33]. Features specific to HCC include arterial phase hypervascularity and late or low washout[34,35]. HCC displays earlier levels of enhancement compared to native liver tissue, and detection rates are greater for larger lesions (2-3 cm) compared to smaller ones (≤ 1 cm)[36]. Within nodules approximately 2 cm or greater, detection rates for ultrasound approach that of CT or MRI. For example, Gaiani *et al*[37] reported a detection rate of 91%-97.3% for evaluating hypervascularity in 103 cirrhotic nodules > 2 cm using CEUS [37]. Limitations of CEUS are like that of conventional ultrasound. Disadvantages of CEUS include user-dependent accuracy, the requirement for multiple contrast injections to survey or investigate separate liver lesions, and restricted ability to distinguish HCC from cholangiocarcinoma and stage disease[34, 38].

EMERGING ADVANCED IMAGING PROTOCOLS

CT and MR perfusion

The acquisition of sequential imaging combined with IV contrast administration by multidetector can permit the assessment of tissue perfusion. The distribution of contrast media between the intravascular and interstitial compartments depends on the extent of blood flow and capillary permeability. Using kinetic models, perfusion parameters across liver tissue can be calculated (blood flow, volume, permeability, hepatic arterial perfusion, portal venous perfusion, perfusion index, slope of increase/decrease). Quantitative color-graded perfusion maps can be used to localize lesions with abnormal tissue perfusion with a high degree of spatial resolution[39-42]. Tumor angiogenesis mediates differences in blood supply between normal liver parenchyma and HCC[42]. Quantitative parameters from CT perfusion, such as hepatic perfusion index, carries high sensitivity and specificity ($\geq 99\%$) for HCC detection in patients with cirrhosis[43]. Early HCC lesions or hepatocellular nodules will demonstrate increased arterial supply as hepatocarcinogenesis progresses, reflected in increased hepatic arterial perfusion and perfusion indices[40]. Other common focal liver lesions can exhibit unique CT perfusion behavior and therefore be used to identify HCC from hemangiomas, liver metastases, and arterioportal shunts[44]. Bai *et al*[45] reported histopathological features such as microvascular density, a poor prognostic factor for HCC, is correlated with multiple perfusion parameters[45]. A major prognostic factor for HCC, microvascular density has been shown to be correlated with multiple CT

perfusion parameters.

Similar to CT perfusion, dynamic contrast-enhanced MRI (DCE-MRI) permits the quantification of perfusion characteristics of liver lesions[46]. This approach is accomplished using gadolinium IV contrast administration followed by image acquisition with high temporal resolution and kinetic modules to quantify contrast distribution perfusion to reflect focal perfusion differences[47]. DCE-MRI perfusion parameters have highlighted unique physiological characteristics in HCC lesions, including increased arterial hepatic blood flow, arterial fraction, and lower portal hepatic blood flow, compared to normal liver parenchyma[46]. Pahwa *et al*[48] reported, arterial fraction and distribution volume are high in HCC and metastatic lesions compared to normal liver parenchyma[48]. Metastatic lesions may also be distinguished from HCC and normal liver parenchyma by the perfusion parameter mean transit time[48]. By evaluating tumor vascularity pre- and post-treatment, DCE-MRI has shown efficacy for treatment monitoring (*e.g.* following administration of anti-angiogenic agents, transarterial chemoembolization or radiotherapy) and predicting survival outcomes for HCC patients[49].

Elastography

Elastography is an imaging method to quantify mechanical properties, notably stiffness, to evaluate focal fibrotic cirrhotic changes (Figure 5). Either MRI or ultrasound, coupled with a device that generates low frequency vibrations (*i.e.* shear waves) and wave propagation, can be quantified in order to calculate levels of stiffness in a focal area of interest[50]. First introduced with ultrasound, there are multiple elastography methods which include transient elastography, point shear wave, two-dimensional shear wave, and quasi-static elastography. Ultrasound elastography has shown to provide satisfactory sensitivity and specificity for identifying histological stages of severe fibrosis (sensitivity: 81.9%, specificity: 84.7%) and cirrhosis (sensitivity: 84.8%, specificity 87.5%)[51]. MRI elastography may also aid to differentiate focal liver lesions. For example, malignant tumors have been reported to have greater levels of stiffness relative to benign lesions, focal fibrotic regions, and normal liver parenchyma [52].

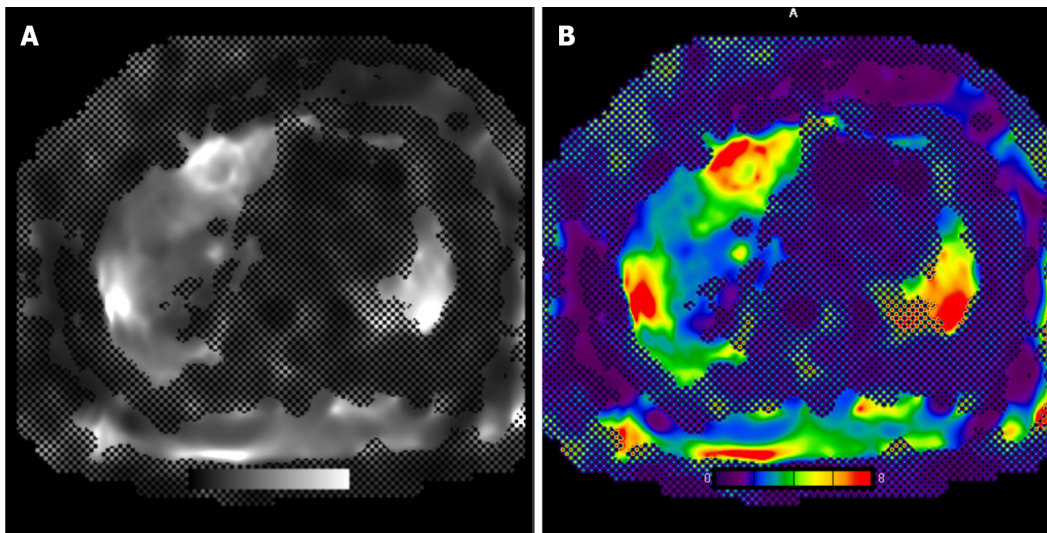
Evaluation of liver stiffness may also offer a prognostic biomarker for determining risk of HCC development and survival. A meta-analysis of 9 studies by Singh *et al*[53] reported increased liver stiffness is associated with an elevated risk of HCC[53]. A more recent meta-analysis of 1735 patients reported a varied sensitivity (31%-100%) and high specificity (81%-94%) for predicting HCC development. The use of MR elastography can also be used as a biomarker to predict treatment response and tumor recurrence[54-56]. A prospective investigation assessed 192 patients undergoing HCC treatment (*e.g.* transarterial chemoembolization, ablation, or resection) found liver parenchymal stiffness to be an independent predictor of early recurrence[54]. A recent investigation also reported efficacy for predicting both early and late recurrence in 180 patients with HBV-related HCC prior to undergoing hepatectomy[56]. Qayyum *et al*[57] reported the use of MR elastography to evaluate stiffness changes in patients treated with immunotherapy (*i.e.* Pembrolizumab). HCC tumor stiffness significantly correlated with survival outcomes, including overall survival and time to disease progression, as well as intratumoral T-lymphocyte abundance[57].

T1 mapping

Similarly, T1 mapping is an MR method by which T1 relaxation time is measured and can be useful for identifying liver fibrosis. In the setting of inflammation and fibrosis, T1 relaxation time will be increased and has been used extensively to evaluate myocardial edema and scarring[58]. In fact, there is a moderate correlation between T1 relaxation time and elastography-measured stiffness[59]. T1 relaxation time can also be measured before and after administering hepatobiliary contrast agents such as GD-EOB-DTPA (Eovist®) to provide a more reliable, quantitative evaluation of contrast media uptake within the liver parenchyma[60]. Given that T1 relaxation is influenced by intrinsic properties of tissue, T1 mapping can overcome some of the traditional limitations of conventional MR signal intensity, which can be influenced by technical factors and imaging parameters. Combining T1 mapping and GD-EOB-DTPA has shown to be useful for identifying and classifying differentiated lesions (*e.g.* reduced uptake associated with increased HCC grade), and can be used to distinguish HCC from other focal liver lesions, including hepatic cysts, focal nodular hyperplasia, and hemangiomas[61-63]. HCCs with microvascular invasion have also shown reductions in T1 relaxation relative to lesions without evidence of microvascular invasion[64], showing promise of another imaging method for predicting prognosis.

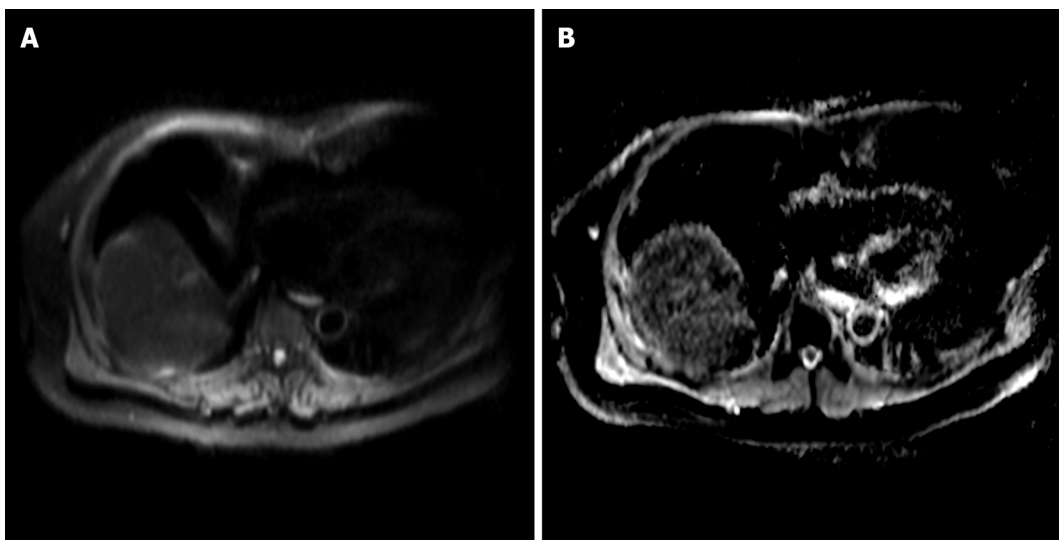
Diffusion weighted imaging

Diffusion weighted imaging (DWI) is a non-invasive MR sequence which can characterize focal liver lesions without the need for contrast media by measuring diffusion properties of water molecules within tissues (Figure 6). Gradations of diffusion are measured using b-values, with greater values denoting more sensitivity to diffusion and higher signal intensity. These values are used to calculate and generate apparent diffusion coefficient (ADC) maps, used clinically to assess local changes in liver tissue diffusion[65]. Changes in cellularity, cell architecture and extracellular space, combined with necrosis and vascularization, can restrict diffusion and thus, HCC will appear hyperintense on DWI[65,66]. DWI has exhibited exceptionally high sensitivity and specificity for a single HCC lesion (100%) and moderate sensitivity and high specificity for multiple lesions (75% and 100%, respectively)[67]. The detection of



DOI: 10.4329/wjr.v15.i3.56 Copyright ©The Author(s) 2023.

Figure 5 Magnetic resonance imaging elastography of the liver. Resonant driver system was used to induce acoustic vibrations in the liver, which were then tracked using magnetic resonance imaging (MRI) scanner to estimate hepatic stiffness. Gray scale and color-scale MRI elastography stiffness sequence. The mean liver stiffness is 4.0 kPa (range: 3.8-4.2 kPa). < 2.5 kPa = Normal; 0.5 to 2.93 kPa = Normal or inflammation; 2.93-3.5 kPa = Stage 1-2 fibrosis; 3.5-4 kPa = Stage 2-3 fibrosis; 4-5 kPa = Stage 3-4 fibrosis; > 5 kPa = Stage 4 or cirrhosis. A: Gray scale; B: Color-scale.



DOI: 10.4329/wjr.v15.i3.56 Copyright ©The Author(s) 2023.

Figure 6 Diffusion-weighted imaging. A: Diffusion-weighted imaging sequence; B: Apparent diffusion coefficient (ADC) map. Increased signal can be observed within the segment VIII lesion with corresponding hypointensity on ADC map, compatible with diffusion restriction.

early, smaller HCC (≤ 2 cm) is a clinically useful feature of DWI, especially when combined with contrast use. Generally, poorly differentiated lesions will exhibit lower ADC compared to well-differentiated lesions[66]. A meta-analysis of 21 studies (1799 HCC lesions) by Surov *et al*[68] reported that DWI can provide grading and prognostic utility by demonstrating use of ADC values can predict tumor grade and microvascular invasiveness (specifically, minimum ADC values)[68]. A recent study in 81 patients with HCC also reported microvascular invasiveness to be associated with ADC with a receiver operating characteristic curve AUC values ranging from 0.860-0.909[69]. DWI has been used as a biomarker for monitoring and predicting tumor response following locoregional therapy[70,71]. ADC correlates with tumor response, according to mRECIST, 6 mo after TACE[70]. ADC values of 1.84×10^{-3} mm²/s10 have been reported to have high sensitivity (92.3%) and specificity values (100%) for identifying evidence of necrosis following TACE[71]. For Y90-radioembolization, increases in ADC value (> 30%) can predict objective mRECIST response with 90% sensitivity and 100% specificity. Further, a > 30% change in ADC following TACE is associated with prolonged overall survival[72]. A prospective investigation of 40 patients treated with radiofrequency ablation found an ADC value of

$1.01 \times 10^{-3} \text{ mm}^2/\text{s}$ yields the highest sensitivity (80%) and specificity (100%) for detecting residual HCCs 3 mo following treatment[73]. However, differentiation between benign and malignant lesions are difficult in the setting of cirrhosis, as the ADC between both lesion types exhibit considerable overlap [65]. Further, standardization for DWI sequences may be needed since different study protocols can alter ADC calculation[74].

MR spectroscopy

MR spectroscopy is an analytical technique that permits the characterization and quantification of tissue metabolite composition *in vivo*. For each given voxel, a plot of signal intensity and metabolites/chemicals are expressed by their frequencies[75]. Malignant hepatic lesions have been found to have elevated choline levels relative to normal liver parenchyma. Changes in metabolite frequencies exist between healthy and cirrhotic livers, namely choline and lipid levels[76]. Choline is a component of phospholipid membranes, which increases in states of cell proliferation and carcinogenesis. Zhang *et al* [77] reported the diagnostic efficacy of measuring choline-containing compounds using MR spectroscopy is high for discriminating malignant and benign tumors (sensitivity: 94.3% and specificity: 93.3%)[77]. Determining ratios of choline and lipids within a given lesion has also been used to monitor treatment responses after locoregional therapy[78]. For example, prospective investigations have found choline levels to decline following TACE therapy[79,80].

Radiogenomics/radiomics

The integration of artificial intelligence and diagnostic imaging modalities has led to an exponential rise in radiogenomics or radiomics, which collectively refers to processes that aim to bridge quantitative radiologic data with immunobiological or clinical characteristics to inform prognosis or predict treatment outcomes[81]. The computing process consists of extracting quantitative features from medical images (CT, MRI or positron emission tomography) into large analyzable databases[82]. This process is carried out in multiple steps, including: (1) Defining volumes or regions of interest; (2) image segmentation (performed manually, semi-automatic or automatic tools); (3) image processing used to normalize grey-level intensities, denoise and improve data quality (*e.g.* signal intensity normalization, motion correction, filtering, image interpolation, and bias field correction); (4) feature extraction; and (5) statistical model building[83,84]. The final process, specific to oncology, includes generating association maps to correlate radiomic-based models with clinical outcome data, microvascular invasion, histological grade, or genomic/molecular data (*e.g.* immune marker expression).

Multiple studies have utilized either radiogenomic or radiomic models to diagnose and differentiate liver tumors or predict treatment efficacy for HCC[85-87]. For example, Lewis *et al*[88] reported greater prediction accuracy when combining LI-RADS and DWI-derived radiomics models using the ADC values than LI-RADS alone for distinguishing HCC from other primary liver cancers[88]. Banerjee *et al* [89] evaluated radiomic-models using contrast-enhanced CT to predict prognostic factors, such as microvascular invasion[89]. Radiogenomic venous invasion, an imaging biomarker, can predict microvascular invasion and correlates with lower overall and recurrence-free survival[89]. A recent meta-analysis/systematic review including 4947 patients showed promising predictive potential of radiomic models for microvascular invasion, reporting a pooled area under the curve (AUC) of 0.85, 0.87, and 0.74 across studies using CT, MR, and ultrasound-based models, respectively[90].

Given the link between gene expression and immunotherapy response, the ability to predict HCC immunoprofiles can be critical for delineating appropriate treatment. Hectors *et al*[91] retrospectively evaluated the relationship between MRI radiomic features (*e.g.* models using tumor size, enhancement ratios, fat content, ADC, texture features) and HCC immunohistochemical and genomic makers[91]. In particular, multiple relationships were found to exist between radiomic features and immunotherapy targets, cytotoxic T-lymphocyte-associated antigen 4 and programmed death 1[91]. Radiomic models have also shown promise for predicting treatment response and potential adverse outcomes after locoregional therapy use[92-96]. For example, MRI-based radiomics models have a reported AUC of 0.861 and 0.884 for predicting tumor response at 3-mo post TACE, evaluated using the mRECIST criterion. While larger, multi-center cohort models should be investigated in the future, the use of radiogenomics or radiomic models provide a novel method that can improve tumor grading, predicting prognosis and clinical decision-making strategies.

CONCLUSION

In summary, the use of imaging is an essential component to the diagnosis and management of HCC. Ultrasound is cost-effective modality for the screening. The utility of diagnostic modalities such as MR or CT for differentiation and grading of HCC continues to expand, especially with the advancement of new techniques and image analyses. The implementation of techniques, including elastography, T1 mapping, perfusion imaging and CEUS provide multiple unique benefits to further aid in the characterization of HCC. Other methods, such as radiomics/radiogenomics, which seek to integrate imaging data to predict prognostic risk factors and determine treatment response probability, will be a new frontier

for informing clinical decision-making with the ultimate goal to generate more precise and personalized treatment management strategies for patients with HCC.

FOOTNOTES

Author contributions: Cody C designed and wrote the review; Nagar AM reviewed and critically advised the paper; Makary MS supervised and critically revised the paper.

Conflict-of-interest statement: All the authors report no relevant conflicts of interest for this article.

Open-Access: This article is an open-access article that was selected by an in-house editor and fully peer-reviewed by external reviewers. It is distributed in accordance with the Creative Commons Attribution NonCommercial (CC BY-NC 4.0) license, which permits others to distribute, remix, adapt, build upon this work non-commercially, and license their derivative works on different terms, provided the original work is properly cited and the use is non-commercial. See: <https://creativecommons.org/licenses/by-nc/4.0/>

Country/Territory of origin: United States

ORCID number: Mina S Makary 0000-0002-2498-7132.

S-Editor: Fan JR

L-Editor: A

P-Editor: Fan JR

REFERENCES

- Villanueva A.** Hepatocellular Carcinoma. *N Engl J Med* 2019; **380**: 1450-1462 [PMID: 30970190 DOI: 10.1056/NEJMra1713263]
- Chakraborty E, Sarkar D.** Emerging Therapies for Hepatocellular Carcinoma (HCC). *Cancers (Basel)* 2022; **14** [PMID: 35681776 DOI: 10.3390/cancers14112798]
- Harris PS, Hansen RM, Gray ME, Massoud OI, McGuire BM, Shoreibah MG.** Hepatocellular carcinoma surveillance: An evidence-based approach. *World J Gastroenterol* 2019; **25**: 1550-1559 [PMID: 30983815 DOI: 10.3748/wjg.v25.i13.1550]
- McGlynn KA, Petrick JL, El-Serag HB.** Epidemiology of Hepatocellular Carcinoma. *Hepatology* 2021; **73** Suppl 1: 4-13 [PMID: 32319693 DOI: 10.1002/hep.31288]
- Parikh ND, Tayob N, Al-Jarrah T, Kramer J, Melcher J, Smith D, Marquardt P, Liu PH, Tang R, Kanwal F, Singal AG.** Barriers to Surveillance for Hepatocellular Carcinoma in a Multicenter Cohort. *JAMA Netw Open* 2022; **5**: e2223504 [PMID: 35867057 DOI: 10.1001/jamanetworkopen.2022.23504]
- Willatt J, Ruma JA, Azar SF, Dasika NL, Syed F.** Imaging of hepatocellular carcinoma and image guided therapies - how we do it. *Cancer Imaging* 2017; **17**: 9 [PMID: 28259177 DOI: 10.1186/s40644-017-0110-z]
- Marrero JA, Kulik LM, Sirlin CB, Zhu AX, Finn RS, Abecassis MM, Roberts LR, Heimbach JK.** Diagnosis, Staging, and Management of Hepatocellular Carcinoma: 2018 Practice Guidance by the American Association for the Study of Liver Diseases. *Hepatology* 2018; **68**: 723-750 [PMID: 29624699 DOI: 10.1002/hep.29913]
- European Association for the Study of the Liver.** EASL Clinical Practice Guidelines: Management of hepatocellular carcinoma. *J Hepatol* 2018; **69**: 182-236 [PMID: 29628281 DOI: 10.1016/j.jhep.2018.03.019]
- Omata M, Cheng AL, Kokudo N, Kudo M, Lee JM, Jia J, Tateishi R, Han KH, Chawla YK, Shiina S, Jafri W, Payawal DA, Ohki T, Ogasawara S, Chen PJ, Lesmana CRA, Lesmana LA, Gani RA, Obi S, Dokmeci AK, Sarin SK.** Asia-Pacific clinical practice guidelines on the management of hepatocellular carcinoma: a 2017 update. *Hepatol Int* 2017; **11**: 317-370 [PMID: 28620797 DOI: 10.1007/s12072-017-9799-9]
- Ahn JC, Lee YT, Agopian VG, Zhu Y, You S, Tseng HR, Yang JD.** Hepatocellular carcinoma surveillance: current practice and future directions. *Hepatoma Res* 2022; **8** [PMID: 36161213 DOI: 10.20517/2394-5079.2021.131]
- Pocha C, Dieperink E, McMaken KA, Knott A, Thuras P, Ho SB.** Surveillance for hepatocellular cancer with ultrasonography vs. computed tomography -- a randomised study. *Aliment Pharmacol Ther* 2013; **38**: 303-312 [PMID: 23750991 DOI: 10.1111/apt.12370]
- Zhang BH, Yang BH, Tang ZY.** Randomized controlled trial of screening for hepatocellular carcinoma. *J Cancer Res Clin Oncol* 2004; **130**: 417-422 [PMID: 15042359 DOI: 10.1007/s00432-004-0552-0]
- Morgan TA, Maturen KE, Dahiya N, Sun MRM, Kamaya A; American College of Radiology Ultrasound Liver Imaging and Reporting Data System (US LI-RADS) Working Group.** US LI-RADS: ultrasound liver imaging reporting and data system for screening and surveillance of hepatocellular carcinoma. *Abdom Radiol (NY)* 2018; **43**: 41-55 [PMID: 28936543 DOI: 10.1007/s00261-017-1317-y]
- Schoenberger H, Chong N, Fetzer DT, Rich NE, Yokoo T, Khatri G, Olivares J, Parikh ND, Yopp AC, Marrero JA, Singal AG.** Dynamic Changes in Ultrasound Quality for Hepatocellular Carcinoma Screening in Patients With Cirrhosis. *Clin Gastroenterol Hepatol* 2022; **20**: 1561-1569.e4 [PMID: 34119640 DOI: 10.1016/j.cgh.2021.06.012]
- Kim SY, An J, Lim YS, Han S, Lee JY, Byun JH, Won HJ, Lee SJ, Lee HC, Lee YS.** MRI With Liver-Specific Contrast for Surveillance of Patients With Cirrhosis at High Risk of Hepatocellular Carcinoma. *JAMA Oncol* 2017; **3**: 456-463 [PMID: 28620797 DOI: 10.1001/jama.2017.1317]

- 27657493 DOI: 10.1001/jamaoncol.2016.3147]
- 16 **Tzartzeva K**, Singal AG. Testing for AFP in combination with ultrasound improves early liver cancer detection. *Expert Rev Gastroenterol Hepatol* 2018; **12**: 947-949 [PMID: 30118333 DOI: 10.1080/17474124.2018.1512855]
 - 17 **Tzartzeva K**, Obi J, Rich NE, Parikh ND, Marrero JA, Yopp A, Waljee AK, Singal AG. Surveillance Imaging and Alpha Fetoprotein for Early Detection of Hepatocellular Carcinoma in Patients With Cirrhosis: A Meta-analysis. *Gastroenterology* 2018; **154**: 1706-1718.e1 [PMID: 29425931 DOI: 10.1053/j.gastro.2018.01.064]
 - 18 **Yilmaz N**, Yilmaz UE, Suer K, Goral V, Cakir N. Screening for hepatocellular carcinoma: summary of current guidelines up to 2018. *Hepatoma Research*. 2018;4:46. DOI:10.20517/2394-5079.2018.49 [DOI: 10.20517/2394-5079.2018.49]
 - 19 **Choi DT**, Kum HC, Park S, Ohsfeldt RL, Shen Y, Parikh ND, Singal AG. Hepatocellular Carcinoma Screening Is Associated With Increased Survival of Patients With Cirrhosis. *Clin Gastroenterol Hepatol* 2019; **17**: 976-987.e4 [PMID: 30616961 DOI: 10.1016/j.cgh.2018.10.031]
 - 20 **Beste LA**, Ioannou GN, Yang Y, Chang MF, Ross D, Dominitz JA. Improved surveillance for hepatocellular carcinoma with a primary care-oriented clinical reminder. *Clin Gastroenterol Hepatol* 2015; **13**: 172-179 [PMID: 24813175 DOI: 10.1016/j.cgh.2014.04.033]
 - 21 **Sherman M**. How to improve HCC surveillance outcomes. *JHEP Rep* 2019; **1**: 460-467 [PMID: 32039398 DOI: 10.1016/j.jhepr.2019.10.007]
 - 22 **Kanmaniraja D**, Dellacerra G, Holder J, Erlichman D, Chernyak V. Liver Imaging Reporting and Data System (LI-RADS) v2018: Review of the CT/MRI Diagnostic Categories. *Can Assoc Radiol J* 2021; **72**: 142-149 [PMID: 32063008 DOI: 10.1177/0846537119888393]
 - 23 **van der Pol CB**, Lim CS, Sirlin CB, McGrath TA, Salameh JP, Bashir MR, Tang A, Singal AG, Costa AF, Fowler K, McInnes MDF. Accuracy of the Liver Imaging Reporting and Data System in Computed Tomography and Magnetic Resonance Image Analysis of Hepatocellular Carcinoma or Overall Malignancy-A Systematic Review. *Gastroenterology* 2019; **156**: 976-986 [PMID: 30445016 DOI: 10.1053/j.gastro.2018.11.020]
 - 24 **Kierans AS**, Song C, Gavlin A, Roudenko A, Lu L, Askin G, Hecht EM. Diagnostic Performance of LI-RADS Version 2018, LI-RADS Version 2017, and OPTN Criteria for Hepatocellular Carcinoma. *AJR Am J Roentgenol* 2020; **215**: 1085-1092 [PMID: 32877248 DOI: 10.2214/AJR.20.22772]
 - 25 **Choi JY**, Lee JM, Sirlin CB. CT and MR imaging diagnosis and staging of hepatocellular carcinoma: part I. Development, growth, and spread: key pathologic and imaging aspects. *Radiology* 2014; **272**: 635-654 [PMID: 25153274 DOI: 10.1148/radiol.14132361]
 - 26 **Kulkarni NM**, Fung A, Kambadakone AR, Yeh BM. Computed Tomography Techniques, Protocols, Advancements, and Future Directions in Liver Diseases. *Magn Reson Imaging Clin N Am* 2021; **29**: 305-320 [PMID: 34243919 DOI: 10.1016/j.mric.2021.05.002]
 - 27 **Hope TA**, Fowler KJ, Sirlin CB, Costa EA, Yee J, Yeh BM, Heiken JP. Hepatobiliary agents and their role in LI-RADS. *Abdom Imaging* 2015; **40**: 613-625 [PMID: 25287679 DOI: 10.1007/s00261-014-0227-5]
 - 28 **Niendorf E**, Spilseth B, Wang X, Taylor A. Contrast Enhanced MRI in the Diagnosis of HCC. *Diagnostics (Basel)* 2015; **5**: 383-398 [PMID: 26854161 DOI: 10.3390/diagnostics5030383]
 - 29 **Schima W**, Heiken J. LI-RADS v2017 for liver nodules: how we read and report. *Cancer Imaging* 2018; **18**: 14 [PMID: 29690933 DOI: 10.1186/s40644-018-0149-5]
 - 30 **Wang G**, Zhu S, Li X. Comparison of values of CT and MRI imaging in the diagnosis of hepatocellular carcinoma and analysis of prognostic factors. *Oncol Lett* 2019; **17**: 1184-1188 [PMID: 30655882 DOI: 10.3892/ol.2018.9690]
 - 31 **Roberts LR**, Sirlin CB, Zaiem F, Almasri J, Prokop LJ, Heimbach JK, Murad MH, Mohammed K. Imaging for the diagnosis of hepatocellular carcinoma: A systematic review and meta-analysis. *Hepatology* 2018; **67**: 401-421 [PMID: 28859233 DOI: 10.1002/hep.29487]
 - 32 **Basha MAA**, AlAzzazy MZ, Ahmed AF, Yousef HY, Shehata SM, El Sammak DAEA, Fathy T, Obaya AA, Abdelbary EH. Does a combined CT and MRI protocol enhance the diagnostic efficacy of LI-RADS in the categorization of hepatic observations? *Eur Radiol* 2018; **28**: 2592-2603 [PMID: 29368164 DOI: 10.1007/s00330-017-5232-y]
 - 33 **Bartolotta TV**, Terranova MC, Gagliardo C, Taibbi A. CEUS LI-RADS: a pictorial review. *Insights Imaging* 2020; **11**: 9 [PMID: 32020352 DOI: 10.1186/s13244-019-0819-2]
 - 34 **Bartolotta TV**, Taibbi A, Midiri M, Lagalla R. Contrast-enhanced ultrasound of hepatocellular carcinoma: where do we stand? *Ultrasonography* 2019; **38**: 200-214 [PMID: 31006227 DOI: 10.14366/usg.18060]
 - 35 **D'Onofrio M**, Crosara S, De Robertis R, Canestrini S, Mucelli RP. Contrast-Enhanced Ultrasound of Focal Liver Lesions. *AJR Am J Roentgenol* 2015; **205**: W56-W66 [PMID: 26102419 DOI: 10.2214/AJR.14.14203]
 - 36 **Zheng SG**, Xu HX, Liu LN. Management of hepatocellular carcinoma: The role of contrast-enhanced ultrasound. *World J Radiol* 2014; **6**: 7-14 [PMID: 24578787 DOI: 10.4329/wjr.v6.i1.7]
 - 37 **Gaiani S**, Celli N, Piscaglia F, Cecilioni L, Losinno F, Giangregorio F, Mancini M, Pini P, Fornari F, Bolondi L. Usefulness of contrast-enhanced perfusional sonography in the assessment of hepatocellular carcinoma hypervascular at spiral computed tomography. *J Hepatol* 2004; **41**: 421-426 [PMID: 15336445 DOI: 10.1016/j.jhep.2004.04.022]
 - 38 **Schwarze V**, Marschner C, Völckers W, Grosu S, Negrão de Figueiredo G, Rübenthaler J, Clevert DA. Diagnostic value of contrast-enhanced ultrasound versus computed tomography for hepatocellular carcinoma: a retrospective, single-center evaluation of 234 patients. *J Int Med Res* 2020; **48**: 300060520930151 [PMID: 32529869 DOI: 10.1177/0300060520930151]
 - 39 **Navin PJ**, Venkatesh SK. Hepatocellular Carcinoma: State of the Art Imaging and Recent Advances. *J Clin Transl Hepatol* 2019; **7**: 72-85 [PMID: 30944823 DOI: 10.14218/JCTH.2018.00032]
 - 40 **Kim SH**, Kamaya A, Willmann JK. CT perfusion of the liver: principles and applications in oncology. *Radiology* 2014; **272**: 322-344 [PMID: 25058132 DOI: 10.1148/radiol.14130091]
 - 41 **Oğul H**, Kantarcı M, Genç B, Pirimoğlu B, Cullu N, Kızrak Y, Yılmaz O, Karabulut N. Perfusion CT imaging of the liver: review of clinical applications. *Diagn Interv Radiol* 2014; **20**: 379-389 [PMID: 24834487 DOI: 10.5152/dir.2014.13396]
 - 42 **Nakamura Y**, Higaki T, Honda Y, Tatsugami F, Tani C, Fukumoto W, Narita K, Kondo S, Akagi M, Awai K. Advanced CT techniques for assessing hepatocellular carcinoma. *Radiol Med* 2021; **126**: 925-935 [PMID: 33954894 DOI: 10.1007/s10156-021-01800-0]

- 10.1007/s11547-021-01366-4]
- 43 **Fischer MA**, Kartalis N, Grigoriadis A, Loizou L, Stål P, Leidner B, Aspelin P, Brismar TB. Perfusion computed tomography for detection of hepatocellular carcinoma in patients with liver cirrhosis. *Eur Radiol* 2015; **25**: 3123-3132 [PMID: 25903707 DOI: 10.1007/s00330-015-3732-1]
 - 44 **Chartampilas E**, Rafailidis V, Georgopoulou V, Kalarakis G, Hatzidakis A, Prassopoulos P. Current Imaging Diagnosis of Hepatocellular Carcinoma. *Cancers (Basel)* 2022; **14** [PMID: 36010991 DOI: 10.3390/cancers14163997]
 - 45 **Bai RJ**, Li JP, Ren SH, Jiang HJ, Liu XD, Ling ZS, Huang Q, Feng GL. A correlation of computed tomography perfusion and histopathology in tumor edges of hepatocellular carcinoma. *Hepatobiliary Pancreat Dis Int* 2014; **13**: 612-617 [PMID: 25475863 DOI: 10.1016/s1499-3872(14)60298-8]
 - 46 **Taouli B**, Johnson RS, Hajdu CH, Oei MT, Merad M, Yee H, Rusinek H. Hepatocellular carcinoma: perfusion quantification with dynamic contrast-enhanced MRI. *AJR Am J Roentgenol* 2013; **201**: 795-800 [PMID: 24059368 DOI: 10.2214/AJR.12.9798]
 - 47 **Aronhime S**, Calcagno C, Jajamovich GH, Dyvorne HA, Robson P, Dieterich D, Fiel MI, Martel-Laferrriere V, Chatterji M, Rusinek H, Taouli B. DCE-MRI of the liver: effect of linear and nonlinear conversions on hepatic perfusion quantification and reproducibility. *J Magn Reson Imaging* 2014; **40**: 90-98 [PMID: 24923476 DOI: 10.1002/jmri.24341]
 - 48 **Pahwa S**, Liu H, Chen Y, Dastmalchian S, O'Connor G, Lu Z, Badve C, Yu A, Wright K, Chalian H, Rao S, Fu C, Vallines I, Griswold M, Seiberlich N, Zeng M, Gulani V. Quantitative perfusion imaging of neoplastic liver lesions: A multi-institution study. *Sci Rep* 2018; **8**: 4990 [PMID: 29563601 DOI: 10.1038/s41598-018-20726-1]
 - 49 **Chen BB**, Shih TT. DCE-MRI in hepatocellular carcinoma-clinical and therapeutic image biomarker. *World J Gastroenterol* 2014; **20**: 3125-3134 [PMID: 24695624 DOI: 10.3748/wjg.v20.i12.3125]
 - 50 **Guglielmo FF**, Venkatesh SK, Mitchell DG. Liver MR Elastography Technique and Image Interpretation: Pearls and Pitfalls. *Radiographics* 2019; **39**: 1983-2002 [PMID: 31626569 DOI: 10.1148/rg.2019190034]
 - 51 **Malik P**, Pillai S, Agarwal K, Abdelwahed S, Bhandari R, Singh A, Chidharla A, Patel K, Singh P, Manaktala P, Rabbani R, Koritala T, Gupta S. Diagnostic Accuracy of Elastography and Liver Disease: A Meta-Analysis. *Gastroenterology Res* 2022; **15**: 232-239 [PMID: 36407808 DOI: 10.14740/gr1557]
 - 52 **Venkatesh SK**, Yin M, Glockner JF, Takahashi N, Araoz PA, Talwalkar JA, Ehman RL. MR elastography of liver tumors: preliminary results. *AJR Am J Roentgenol* 2008; **190**: 1534-1540 [PMID: 18492904 DOI: 10.2214/AJR.07.3123]
 - 53 **Singh S**, Fujii LL, Murad MH, Wang Z, Asrani SK, Ehman RL, Kamath PS, Talwalkar JA. Liver stiffness is associated with risk of decompensation, liver cancer, and death in patients with chronic liver diseases: a systematic review and meta-analysis. *Clin Gastroenterol Hepatol* 2013; **11**: 1573-84.e1 [PMID: 23954643 DOI: 10.1016/j.cgh.2013.07.034]
 - 54 **Cho HJ**, Kim B, Kim HJ, Huh J, Kim JK, Lee JH, Seo CW, Ahn HR, Eun JW, Kim SS, Cho SW, Cheong JY. Liver stiffness measured by MR elastography is a predictor of early HCC recurrence after treatment. *Eur Radiol* 2020; **30**: 4182-4192 [PMID: 32189053 DOI: 10.1007/s00330-020-06792-y]
 - 55 **Gordic S**, Ayache JB, Kennedy P, Besa C, Wagner M, Bane O, Ehman RL, Kim E, Taouli B. Value of tumor stiffness measured with MR elastography for assessment of response of hepatocellular carcinoma to locoregional therapy. *Abdom Radiol (NY)* 2017; **42**: 1685-1694 [PMID: 28154910 DOI: 10.1007/s00261-017-1066-y]
 - 56 **Zhang L**, Chen J, Jiang H, Rong D, Guo N, Yang H, Zhu J, Hu B, He B, Yin M, Venkatesh SK, Ehman RL, Wang J. MR elastography as a biomarker for prediction of early and late recurrence in HBV-related hepatocellular carcinoma patients before hepatectomy. *Eur J Radiol* 2022; **152**: 110340 [PMID: 35580445 DOI: 10.1016/j.ejrad.2022.110340]
 - 57 **Qayyum A**, Hwang KP, Stafford J, Verma A, Maru DM, Sandesh S, Sun J, Pestana RC, Avritscher R, Hassan MM, Amin H, Rashid A, Wistuba IL, Ehman RL, Ma J, Kaseb AO. Immunotherapy response evaluation with magnetic resonance elastography (MRE) in advanced HCC. *J Immunother Cancer* 2019; **7**: 329 [PMID: 31779702 DOI: 10.1186/s40425-019-0766-y]
 - 58 **Taylor AJ**, Salerno M, Dharmakumar R, Jerosch-Herold M. T1 Mapping: Basic Techniques and Clinical Applications. *JACC Cardiovasc Imaging* 2016; **9**: 67-81 [PMID: 26762877 DOI: 10.1016/j.jcmg.2015.11.005]
 - 59 **Hoffman DH**, Ayoola A, Nickel D, Han F, Chandarana H, Shanbhogue KP. T1 mapping, T2 mapping and MR elastography of the liver for detection and staging of liver fibrosis. *Abdom Radiol (NY)* 2020; **45**: 692-700 [PMID: 31875241 DOI: 10.1007/s00261-019-02382-9]
 - 60 **Katsube T**, Okada M, Kumano S, Hori M, Imaoka I, Ishii K, Kudo M, Kitagaki H, Murakami T. Estimation of liver function using T1 mapping on Gd-EOB-DTPA-enhanced magnetic resonance imaging. *Invest Radiol* 2011; **46**: 277-283 [PMID: 21343827 DOI: 10.1097/RLI.0b013e318200f67d]
 - 61 **Peng Z**, Jiang M, Cai H, Chan T, Dong Z, Luo Y, Li ZP, Feng ST. Gd-EOB-DTPA-enhanced magnetic resonance imaging combined with T1 mapping predicts the degree of differentiation in hepatocellular carcinoma. *BMC Cancer* 2016; **16**: 625 [PMID: 27520833 DOI: 10.1186/s12885-016-2607-4]
 - 62 **Peng Z**, Li C, Chan T, Cai H, Luo Y, Dong Z, Li ZP, Feng ST. Quantitative evaluation of Gd-EOB-DTPA uptake in focal liver lesions by using T1 mapping: differences between hepatocellular carcinoma, hepatic focal nodular hyperplasia and cavernous hemangioma. *Oncotarget* 2017; **8**: 65435-65444 [PMID: 29029443 DOI: 10.18632/oncotarget.18918]
 - 63 **Mio M**, Fujiwara Y, Tani K, Toyofuku T, Maeda T, Inoue T. Quantitative evaluation of focal liver lesions with T1 mapping using a phase-sensitive inversion recovery sequence on gadoxetic acid-enhanced MRI. *Eur J Radiol Open* 2021; **8**: 100312 [PMID: 33392362 DOI: 10.1016/j.ejro.2020.100312]
 - 64 **Rao C**, Wang X, Li M, Zhou G, Gu H. Value of T1 mapping on gadoxetic acid-enhanced MRI for microvascular invasion of hepatocellular carcinoma: a retrospective study. *BMC Med Imaging* 2020; **20**: 43 [PMID: 32345247 DOI: 10.1186/s12880-020-00433-y]
 - 65 **Kele PG**, van der Jagt EJ. Diffusion weighted imaging in the liver. *World J Gastroenterol* 2010; **16**: 1567-1576 [PMID: 20355235 DOI: 10.3748/wjg.v16.i13.1567]
 - 66 **Saito K**, Tajima Y, Harada TL. Diffusion-weighted imaging of the liver: Current applications. *World J Radiol* 2016; **8**: 857-867 [PMID: 27928467 DOI: 10.4329/wjr.v8.i11.857]
 - 67 **Shankar S**, Kalra N, Bhatia A, Srinivasan R, Singh P, Dhiman RK, Khandelwal N, Chawla Y. Role of Diffusion Weighted Imaging (DWI) for Hepatocellular Carcinoma (HCC) Detection and its Grading on 3T MRI: A Prospective Study. *J Clin*

- Exp Hepatol* 2016; **6**: 303-310 [PMID: 28003720 DOI: 10.1016/j.jceh.2016.08.012]
- 68 **Surov A**, Pech M, Omari J, Fischbach F, Damm R, Fischbach K, Powerski M, Relja B, Wienke A. Diffusion-Weighted Imaging Reflects Tumor Grading and Microvascular Invasion in Hepatocellular Carcinoma. *Liver Cancer* 2021; **10**: 10-24 [PMID: 33708636 DOI: 10.1159/000511384]
- 69 **Jing M**, Cao Y, Zhang P, Zhang B, Lin X, Deng L, Han T, Zhou J. The Benefit of Apparent Diffusion Coefficient in Evaluating the Invasiveness of Hepatocellular Carcinoma. *Front Oncol* 2021; **11**: 719480 [PMID: 34504795 DOI: 10.3389/fonc.2021.719480]
- 70 **Ludwig JM**, Camacho JC, Kokabi N, Xing M, Kim HS. The Role of Diffusion-Weighted Imaging (DWI) in Locoregional Therapy Outcome Prediction and Response Assessment for Hepatocellular Carcinoma (HCC): The New Era of Functional Imaging Biomarkers. *Diagnostics (Basel)* 2015; **5**: 546-563 [PMID: 26854170 DOI: 10.3390/diagnostics5040546]
- 71 **Yuan Z**, Zhang J, Yang H, Ye XD, Xu LC, Li WT. Diffusion-Weighted MR Imaging of Hepatocellular Carcinoma: Current Value in Clinical Evaluation of Tumor Response to Locoregional Treatment. *J Vasc Interv Radiol* 2016; **27**: 20-30; quiz 31 [PMID: 26621785 DOI: 10.1016/j.jvir.2015.10.003]
- 72 **Kokabi N**, Camacho JC, Xing M, Qiu D, Kitajima H, Mittal PK, Kim HS. Apparent diffusion coefficient quantification as an early imaging biomarker of response and predictor of survival following yttrium-90 radioembolization for unresectable infiltrative hepatocellular carcinoma with portal vein thrombosis. *Abdom Imaging* 2014; **39**: 969-978 [PMID: 24740759 DOI: 10.1007/s00261-014-0127-8]
- 73 **Elrefaey Hasan BM**, Abd ElHamid HAE, Khater NH, ElGendy W, Abdelrahman AS. Role of DWI in evaluation of HCC after radiofrequency ablation compared to dynamic MRI using MRI (3 T). *Egyptian J Radiol Nucl Med* 2021; **52**: 267 [DOI: 10.1186/s43055-021-00647-2]
- 74 **Granata V**, Fusco R, Filice S, Incollingo P, Belli A, Izzo F, Petrillo A. Comment on "State of the art in magnetic resonance imaging of hepatocellular carcinoma": the role of DWI. *Radiol Oncol* 2019; **53**: 369-370 [PMID: 31318697 DOI: 10.2478/raon-2019-0031]
- 75 **Qayyum A**. MR spectroscopy of the liver: principles and clinical applications. *Radiographics* 2009; **29**: 1653-1664 [PMID: 19959513 DOI: 10.1148/rg.296095520]
- 76 **Wang D**, Li Y. 1H Magnetic Resonance Spectroscopy Predicts Hepatocellular Carcinoma in a Subset of Patients With Liver Cirrhosis: A Randomized Trial. *Medicine (Baltimore)* 2015; **94**: e1066 [PMID: 26166077 DOI: 10.1097/MD.0000000000001066]
- 77 **Zhang L**, Zhao X, Ouyang H, Wang S, Zhou C. Diagnostic value of 3.0T (1)H MRS with choline-containing compounds ratio (ΔCC) in primary malignant hepatic tumors. *Cancer Imaging* 2016; **16**: 25 [PMID: 27549094 DOI: 10.1186/s40644-016-0082-4]
- 78 **Yang K**, Zhang XM, Yang L, Xu H, Peng J. Advanced imaging techniques in the therapeutic response of transarterial chemoembolization for hepatocellular carcinoma. *World J Gastroenterol* 2016; **22**: 4835-4847 [PMID: 27239110 DOI: 10.3748/wjg.v22.i20.4835]
- 79 **Kuo YT**, Li CW, Chen CY, Jao J, Wu DK, Liu GC. In vivo proton magnetic resonance spectroscopy of large focal hepatic lesions and metabolite change of hepatocellular carcinoma before and after transcatheter arterial chemoembolization using 3.0-T MR scanner. *J Magn Reson Imaging* 2004; **19**: 598-604 [PMID: 15112309 DOI: 10.1002/jmri.20046]
- 80 **Chen CY**, Li CW, Kuo YT, Jaw TS, Wu DK, Jao JC, Hsu JS, Liu GC. Early response of hepatocellular carcinoma to transcatheter arterial chemoembolization: choline levels and MR diffusion constants--initial experience. *Radiology* 2006; **239**: 448-456 [PMID: 16569781 DOI: 10.1148/radiol.2392042202]
- 81 **Jeong WK**, Jamshidi N, Felker ER, Raman SS, Lu DS. Radiomics and radiogenomics of primary liver cancers. *Clin Mol Hepatol* 2019; **25**: 21-29 [PMID: 30441889 DOI: 10.3350/cmh.2018.1007]
- 82 **Gillies RJ**, Kinahan PE, Hricak H. Radiomics: Images Are More than Pictures, They Are Data. *Radiology* 2016; **278**: 563-577 [PMID: 26579733 DOI: 10.1148/radiol.2015151169]
- 83 **Shur JD**, Doran SJ, Kumar S, Ap Dafydd D, Downey K, O'Connor JPB, Papanikolaou N, Messiou C, Koh DM, Orton MR. Radiomics in Oncology: A Practical Guide. *Radiographics* 2021; **41**: 1717-1732 [PMID: 34597235 DOI: 10.1148/rg.2021210037]
- 84 **van Timmeren JE**, Cester D, Tanadini-Lang S, Alkadhi H, Baessler B. Radiomics in medical imaging--"how-to" guide and critical reflection. *Insights Imaging* 2020; **11**: 91 [PMID: 32785796 DOI: 10.1186/s13244-020-00887-2]
- 85 **Gong XQ**, Tao YY, Wu YK, Liu N, Yu X, Wang R, Zheng J, Huang XH, Li JD, Yang G, Wei XQ, Yang L, Zhang XM. Progress of MRI Radiomics in Hepatocellular Carcinoma. *Front Oncol* 2021; **11**: 698373 [PMID: 34616673 DOI: 10.3389/fonc.2021.698373]
- 86 **Fu J**, Cao SJ, Song L, Tong XQ, Wang J, Yang M, Zou YH. Radiomics/Radiogenomics in hepatocellular carcinoma: Applications and challenges in interventional management. *iLIVER* 2022; **1**: 96-100 [DOI: 10.1016/j.iliver.2022.07.001]
- 87 **Yao S**, Ye Z, Wei Y, Jiang HY, Song B. Radiomics in hepatocellular carcinoma: A state-of-the-art review. *World J Gastrointest Oncol* 2021; **13**: 1599-1615 [PMID: 34853638 DOI: 10.4251/wjgo.v13.i11.1599]
- 88 **Lewis S**, Peti S, Hectors SJ, King M, Rosen A, Kamath A, Putra J, Thung S, Taouli B. Volumetric quantitative histogram analysis using diffusion-weighted magnetic resonance imaging to differentiate HCC from other primary liver cancers. *Abdom Radiol (NY)* 2019; **44**: 912-922 [PMID: 30712136 DOI: 10.1007/s00261-019-01906-7]
- 89 **Banerjee S**, Wang DS, Kim HJ, Sirlin CB, Chan MG, Korn RL, Rutman AM, Siripongsakun S, Lu D, Imanbayev G, Kuo MD. A computed tomography radiogenomic biomarker predicts microvascular invasion and clinical outcomes in hepatocellular carcinoma. *Hepatology* 2015; **62**: 792-800 [PMID: 25930992 DOI: 10.1002/hep.27877]
- 90 **Zhong X**, Long H, Su L, Zheng R, Wang W, Duan Y, Hu H, Lin M, Xie X. Radiomics models for preoperative prediction of microvascular invasion in hepatocellular carcinoma: a systematic review and meta-analysis. *Abdom Radiol (NY)* 2022; **47**: 2071-2088 [PMID: 35364684 DOI: 10.1007/s00261-022-03496-3]
- 91 **Hectors SJ**, Lewis S, Besa C, King MJ, Said D, Putra J, Ward S, Higashi T, Thung S, Yao S, Laface I, Schwartz M, Gnjatic S, Merad M, Hoshida Y, Taouli B. MRI radiomics features predict immuno-oncological characteristics of hepatocellular carcinoma. *Eur Radiol* 2020; **30**: 3759-3769 [PMID: 32086577 DOI: 10.1007/s00330-020-06675-2]
- 92 **Niu XK**, He XF. Development of a computed tomography-based radiomics nomogram for prediction of transarterial

- chemoembolization refractoriness in hepatocellular carcinoma. *World J Gastroenterol* 2021; **27**: 189-207 [PMID: 33510559 DOI: 10.3748/wjg.v27.i2.189]
- 93 **Kong C**, Zhao Z, Chen W, Lv X, Shu G, Ye M, Song J, Ying X, Weng Q, Weng W, Fang S, Chen M, Tu J, Ji J. Prediction of tumor response via a pretreatment MRI radiomics-based nomogram in HCC treated with TACE. *Eur Radiol* 2021; **31**: 7500-7511 [PMID: 33860832 DOI: 10.1007/s00330-021-07910-0]
- 94 **Sheen H**, Kim JS, Lee JK, Choi SY, Baek SY, Kim JY. A radiomics nomogram for predicting transcatheter arterial chemoembolization refractoriness of hepatocellular carcinoma without extrahepatic metastasis or macrovascular invasion. *Abdom Radiol (NY)* 2021; **46**: 2839-2849 [PMID: 33388805 DOI: 10.1007/s00261-020-02884-x]
- 95 **Bai H**, Meng S, Xiong C, Liu Z, Shi W, Ren Q, Xia W, Zhao X, Jian J, Song Y, Ni C, Gao X, Li Z. Preoperative CECT-based Radiomic Signature for Predicting the Response of Transarterial Chemoembolization (TACE) Therapy in Hepatocellular Carcinoma. *Cardiovasc Intervent Radiol* 2022; **45**: 1524-1533 [PMID: 35896687 DOI: 10.1007/s00270-022-03221-z]
- 96 **Zhao Y**, Wang N, Wu J, Zhang Q, Lin T, Yao Y, Chen Z, Wang M, Sheng L, Liu J, Song Q, Wang F, An X, Guo Y, Li X, Wu T, Liu AL. Radiomics Analysis Based on Contrast-Enhanced MRI for Prediction of Therapeutic Response to Transarterial Chemoembolization in Hepatocellular Carcinoma. *Front Oncol* 2021; **11**: 582788 [PMID: 33868988 DOI: 10.3389/fonc.2021.582788]

Multi-modality parathyroid imaging: A shifting paradigm

Shrea Gulati, Sunil Chumber, Gopal Puri, Stanzin Spalkit, N A Damle, CJ Das

Specialty type: Radiology, nuclear medicine and medical imaging

Provenance and peer review: Invited article; Externally peer reviewed.

Peer-review model: Single blind

Peer-review report's scientific quality classification

Grade A (Excellent): 0
Grade B (Very good): 0
Grade C (Good): C, C
Grade D (Fair): 0
Grade E (Poor): 0

P-Reviewer: Nambi G, Saudi Arabia; Wu SZ, China

Received: December 24, 2022

Peer-review started: December 24, 2022

First decision: January 3, 2023

Revised: January 20, 2023

Accepted: March 1, 2023

Article in press: March 1, 2023

Published online: March 28, 2023



Shrea Gulati, Stanzin Spalkit, CJ Das, Department of Radiodiagnosis and Interventional Radiology, All India Institute of Medical Sciences, New Delhi 110029, Delhi, India

Sunil Chumber, Gopal Puri, Department of Surgical Disciplines, All India Institute of Medical Sciences, New Delhi 110029, Delhi, India

N A Damle, Department of Nuclear Medicine, All India Institute of Medical Sciences, New Delhi 110029, Delhi, India

Corresponding author: CJ Das, FRCP, MBBS, MD, Professor, Department of Radiodiagnosis and Interventional Radiology, All India Institute of Medical Sciences, Aurobindo Marg Ansari Nagar, New Delhi 110029, Delhi, India. docchandan17@gmail.com

Abstract

The goal of parathyroid imaging in hyperparathyroidism is not diagnosis, rather it is the localization of the cause of hyperparathyroidism for planning the best therapeutic approach. Hence, the role of imaging to accurately and precisely localize the abnormal parathyroid tissue is more important than ever to facilitate minimally invasive parathyroidectomy over bilateral neck exploration. The common causes include solitary parathyroid adenoma, multiple parathyroid adenomas, parathyroid hyperplasia and parathyroid carcinoma. It is highly imperative for the radiologist to be cautious of the mimics of parathyroid lesions like thyroid nodules and lymph nodes and be able to differentiate them on imaging. The various imaging modalities available include high resolution ultrasound of the neck, nuclear imaging studies, four-dimensional computed tomography (4D CT) and magnetic resonance imaging. Contrast enhanced ultrasound is a novel technique which has been recently added to the armamentarium to differentiate between parathyroid adenomas and its mimics. Through this review article we wish to review the imaging features of parathyroid lesions on various imaging modalities and present an algorithm to guide their radiological differentiation from mimics.

Key Words: Parathyroid adenoma; Ultrasound; Four-dimensional computed tomography; Magnetic resonance imaging; Nuclear Imaging; Contrast enhanced ultrasound

©The Author(s) 2023. Published by Baishideng Publishing Group Inc. All rights reserved.

Core Tip: Parathyroid adenoma is the commonest cause of primary hyperparathyroidism, the management of which lies in definitive surgery. Accurate preoperative imaging is of prime importance to facilitate surgery. Imaging modalities include radiological investigations like ultrasound, four-dimensional computed tomography and magnetic resonance imaging which provide anatomical localization and nuclear scans like MIBI, single photon emission computed tomography and Fluoro-choline positron emission tomography which provide functional imaging details. Contrast-enhanced ultrasound is a novel modality which is being explored in the evaluation of parathyroid adenomas.

Citation: Gulati S, Chumber S, Puri G, Spalkit S, Damle NA, Das CJ. Multi-modality parathyroid imaging: A shifting paradigm. *World J Radiol* 2023; 15(3): 69-82

URL: <https://www.wjgnet.com/1949-8470/full/v15/i3/69.htm>

DOI: <https://dx.doi.org/10.4329/wjr.v15.i3.69>

INTRODUCTION

Primary hyperparathyroidism is the commonest cause of hypercalcemia resulting from pathologies intrinsic to the parathyroid glands[1]. It manifests biochemically as raised parathyroid hormone and calcium levels[2]. Primary hyperparathyroidism is most commonly due to a single benign parathyroid adenoma (approximately 80% of the patients), with multiglandular disease seen in approximately 15%-20% of patients[3]. Primary hyperparathyroidism is due to multiglandular involvement consisting of either multiple adenomas or hyperplasia of all 4 glands (5%-10%) and very rarely by parathyroid carcinoma (< 1%)[4]. The definitive management is achieved by surgical excision of the abnormal parathyroid tissue. Preoperative imaging is mandatory in deciding the surgical approach and improves localisation of the abnormal gland. The commonly accepted modalities to guide imaging include ultrasound, 4-dimensional computed tomography (4D CT), magnetic resonance imaging (MRI) and nuclear medicine studies whereas contrast-enhanced ultrasound (CEUS) is the new kid on the block. In this review, we would like to revisit the characteristic imaging findings on various modalities and will present an algorithm of differentiating parathyroid adenomas from their mimics.

ANATOMY

The usual number of parathyroid glands is four, but this can vary. Some persons have more than four parathyroid glands. The normal shape of the parathyroid gland is ovoid or bean shaped and it measures 4-6 mm in length, 2-4 mm in width and 1-2 mm in thickness. The plane of the recurrent laryngeal nerve (RLN), identified by the trachea-oesophageal groove helps identify the superior and inferior parathyroid glands, the superior is posterior to the RLN while the inferior is anterior to the RLN[5]. In 16 % of the individuals the parathyroid glands are ectopically located[6]. The embryological origin of the inferior parathyroid glands is from the third pharyngeal pouch while the origin of the superior parathyroid gland is from the fourth pharyngeal pouch. The longer course of embryological migration of the superior parathyroid glands makes it more prone for ectopic location. Ectopic superior parathyroid glands are found in the retropharyngeal or retroesophageal locations, while ectopic inferior parathyroid glands may be seen within the carotid sheath or mediastinum (Figure 1)[7]. Uncommonly, there may be failure of descent of the inferior parathyroid glands, which may be finally located cephalad to the superior parathyroid glands[8].

ROLE OF IMAGING

The diagnosis of primary hyperparathyroidism is made biochemically with demonstration of raised parathormone (PTH) levels. The role of radiology in hyperparathyroidism is not diagnosis, rather it is accurate localisation and surgical planning[5]. There are two approaches to surgical management of hyperparathyroidism - bilateral neck exploration (BNE) and minimally invasive parathyroidectomy (MIP). BNE is the conventional surgical approach which involves a large midline surgical incision, exploration and examination of all four parathyroid glands and excision of the abnormal tissue. Due to the large incision involved and meticulous exploration, it is associated with excellent long term cure rates[9]. The downside of this meticulousness is the associated higher risk of recurrent laryngeal nerve damage and poor cosmesis. MIP involves a unilateral small incision on the affected side and surgical removal of only the pathological gland identified precisely and accurately by preoperative imaging studies[5]. As per the European Society of Endocrine Surgeons, in experienced hands, keeping in view

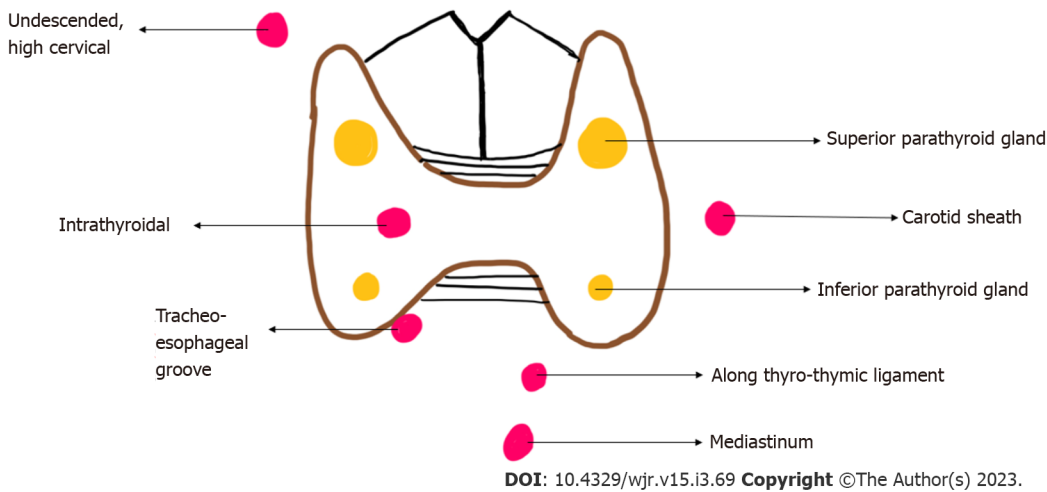


Figure 1 Diagrammatic representation of location of eutopic (yellow) and ectopic (red) parathyroid glands.

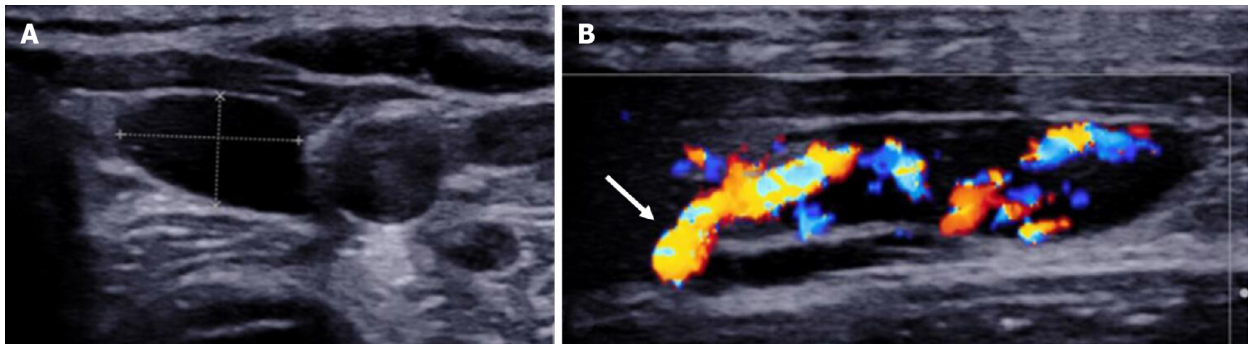


Figure 2 Left inferior parathyroid adenoma. A: High resolution ultrasound image of the neck in the transverse plane demonstrates a well-circumscribed homogeneously hypoechoic ovoid lesion located at the lower pole of the left lobe of thyroid gland; B: Colour Doppler shows a big feeding vessel, likely from the inferior thyroid artery (arrow) supplying the lesion.

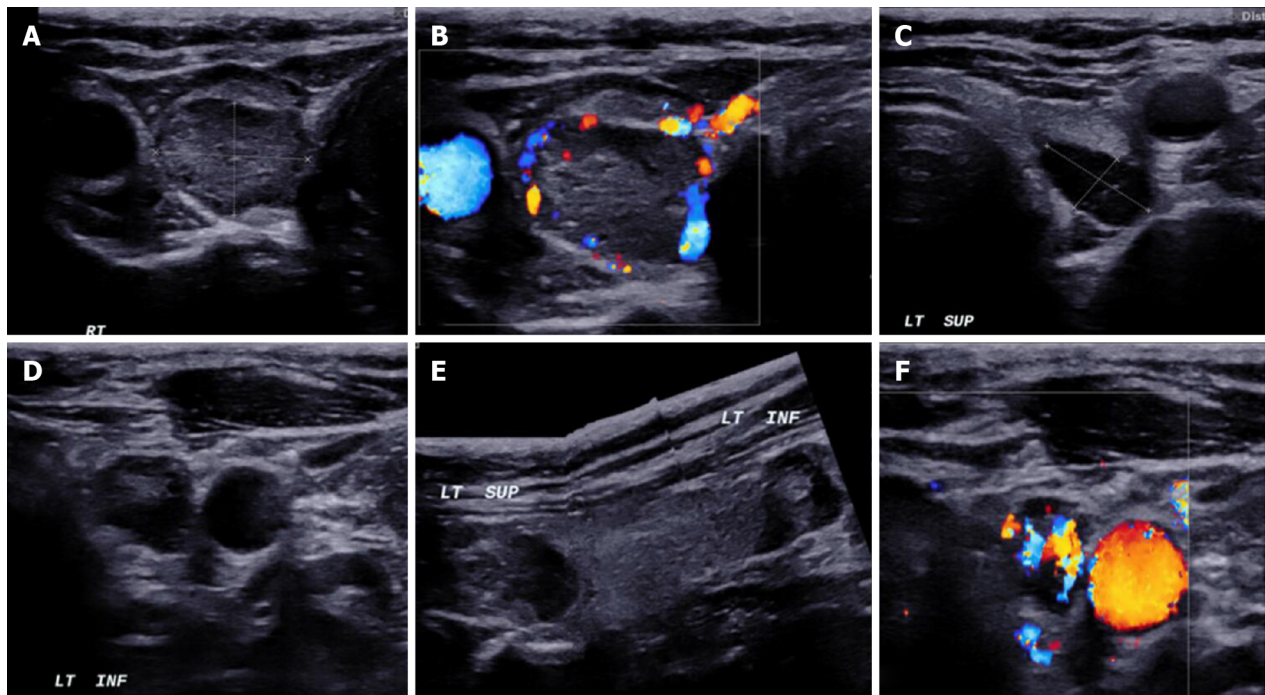
the indications and contraindications of the surgery, MIP is a reliable and safe procedure with equivalent cure rates[9]. As compared to BNE, MIP is associated with shorter operative times, better cosmesis, shorter hospital stays and therefore lower costs[10].

IMAGING

The imaging techniques available for parathyroid imaging include high resolution ultrasound of the neck, Tc99m sestamibi scan, 4D CT and MRI.

HIGH RESOLUTION ULTRASONOGRAPHY

Duplex ultrasound with a linear array transducer with 10 MHz or higher frequency is used for imaging of the parathyroid glands. With the patient in supine position and mild neck extension (using a pillow under the upper back), the neck is scanned in both transverse and longitudinal planes focusing on the region behind the thyroid gland. The normal location of parathyroid glands lesions is lateral to the trachea and oesophagus and medial to the carotid artery and the jugular vein. This knowledge helps to closely inspect the expected locations meanwhile differentiating it from close mimics. The small size and deep location of the normal parathyroid gland makes it non-identifiable on ultrasound. Parathyroid adenomas which are larger than 1 cm in size are readily visible on ultrasound. The sonographic detection of small parathyroid adenomas, especially those < 1 cm in size can be enhanced by using graded compression technique[11]. Parathyroid adenomas are oval/bean shaped, well circumscribed lesions which are homogeneously hypoechoic as compared to the neighbouring thyroid gland (Figure 2). Color Doppler provides associate information of the origin and course of the feeding artery of the



DOI: 10.4329/wjr.v15.i3.69 Copyright ©The Author(s) 2023.

Figure 3 In a patient with MEN-1 syndrome. A-F: Ultrasound neck images show multiple (3) parathyroid adenoma in the right superior and left superior and inferior parathyroid glands respectively.

parathyroid adenoma[12,13]. This is attributed to the high vascularity of the parathyroid adenomas which are supplied by an enlarged feeding inferior thyroidal artery (Feeding vessel sign). Spectral Doppler can determine the blood flow velocity of the feeding artery and get information of a low resistive index. This polar vascularity sign helps in differentiation from a lymph node which typically shows central hilar vascularity on Doppler[14]. Along with hypervascularity of the affected parathyroid, the ipsilateral thyroid gland can also show hyperaemia in 85% of the cases and this may serve as a surrogate marker of underlying parathyroid adenoma[11,14]. In patients with known syndromes like MEN-1 (Figure 3), multiple adenomas can be seen and identification of a single adenoma should not lead to a false sense of satisfaction of search. Uncommonly, parathyroid adenomas can show atypical features such as ectopic location, completely intrathyroidal location, internal areas of cystic degeneration, heterogenous internal echotexture rather than the homogenous hypoechoic echotexture which make prospective sonographic diagnosis difficult[15-18].

High resolution ultrasound has the advantage of non-involvement of radiation, low cost and easy availability. Although ultrasound is highly operator dependant in the detection of parathyroid adenomas, it has a sensitivity of 84% in the hands of an experienced sonologist[19]. The two most important differentials of parathyroid adenomas are thyroid nodules and lymph nodes, and ultrasound is a useful modality for their differentiation (Table 1). The oesophagus and the longus colli muscle can sometimes mimic parathyroid adenomas[14].

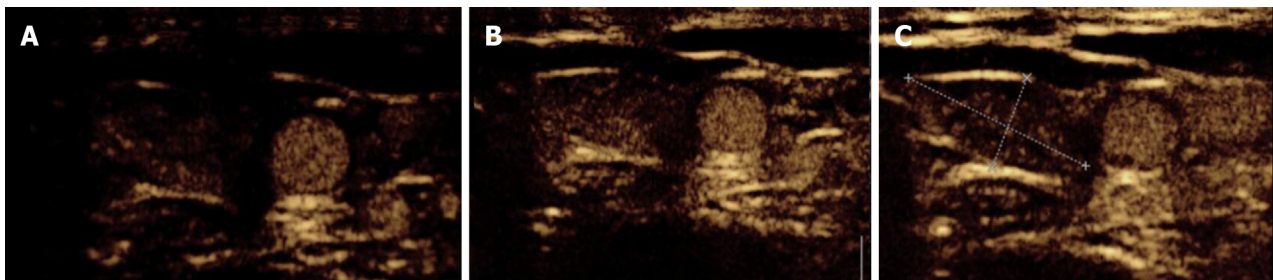
CEUS

CEUS is the new armamentarium added in the evaluation of parathyroid adenomas. The differentiation of parathyroid adenomas from parathyroid hyperplasia as well as non-parathyroid lesions like lymph nodes and thyroid nodules is difficult on conventional ultrasound[7,20]. Studies have demonstrated the use of contrast enhanced ultrasound as a novel technique in the differentiation of these entities[21-23]. On CEUS, parathyroid adenomas show early peripheral hyperenhancement with central washout in the later phases (Figure 4)[21]. Parathyroid hyperplasia on the other hand shows more homogenous contrast uptake[21]. Physiological lymph nodes show homogenous and centrifugal pattern of enhancement[24-26]. Thyroid nodules tend to show homogenous hyperenhancement with a fast wash-in and slow washout pattern[21].

Table 1 Differentiating features of parathyroid adenoma from lymph nodes and thyroid nodules on imaging

Modality	Features	Parathyroid adenoma	Thyroid nodule	Lymph node
USG	Echogenicity	Homogenously markedly hypoechoic	Homo/Heterogenously hypo/isoechoic	Central echogenic hilum
	Vascularity	Peripheral polar vessel sign present	Not seen	Central/hilar vascularity
	Calcification	Less common	Common	+/-
	Cystic changes	Less common	More common	+/-
CT	Non contrast	Hypodense	Hyperdense	Hypodense
	Arterial	Intense arterial enhancement	Enhancement in arterial phase but less than parathyroid adenomas	No enhancement in the arterial phase
	Venous	Washout	Persistent enhancement	Progressive enhancement in venous phase
MRI	Morphology	Cleavage plane with thyroid gland	No cleavage plane	Cleavage plane present
	Diffusion weighted Image	High SI		High SI
PET Choline	Uptake	Present	Variable	Uptake may be present, however is delayed and of lesser intensity

USG: Ultrasound; CT: Computed tomography; MRI: Magnetic resonance imaging; SI: Signal intensity; PET: Positron emission tomography.



DOI: 10.4329/wjr.v15.i3.69 Copyright ©The Author(s) 2023.

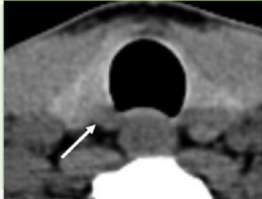
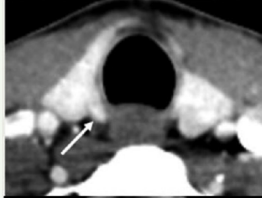
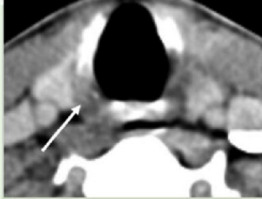
Figure 4 Contrast-enhanced ultrasound in parathyroid adenoma. A-C: A 33-year-old female with raised parathormone levels (87 IU) was assessed using contrast enhanced ultrasound. A circumscribed lesion at the lower pole of the left lobe of thyroid gland was found consistent with parathyroid adenoma, demonstrating early peripheral enhancement with central washout.

SHEAR WAVE ELASTOGRAPHY

This is a newer modality which has been explored for distinguishing parathyroid adenoma from the neighbouring thyroid tissue. Parathyroid adenomas show a significantly lower tissue elasticity than thyroid tissue. This may serve as an additional differentiating feature between the two entities[27].

PARATHYROID SCINTIGRAPHY

The most common radiotracer used for imaging parathyroid glands is sestamibi with ^{99m}Tc . Both thyroid and parathyroid glands take up sestamibi, however the differentiating point is that the uptake by hyperplastic or adenomatous parathyroid tissue is more intense, and also shows a delayed wash-out as compared to thyroid tissue which shows faster wash-out[28]. Therefore, foci of increased radiotracer uptake persisting on a delayed scan (variably acquired at 60-180 min after radio-tracer administration) represents parathyroid tissue. Subtracting images acquired by using two radio-tracer agents, the first one which is taken up by both thyroid and parathyroid tissue (like sestamibi) and a second which is taken up by only thyroid tissue (^{99m}Tc pertechnetate or ^{123}I) can help image the parathyroid. This was the basis of the famous Thallium- Technetium subtraction scan. However, this technique is less used these days due to the availability of more effective radiotracer, sestamibi.

S no.	Phase of CT	Region scanned	Time delay after start of contrast injection	Imaging features	Representative image
1	Non-contrast	Hyoid bone to clavicle	-	Hypodense (as compared to the thyroid gland which is hyperdense)	
2	Arterial phase	Angle of mandible to carina	25 s	Hyperenhancement on the arterial phase	
3	Delayed (venous phase)	Angle of mandible to carina	80 s	Washout on the venous phase	

DOI: 10.4329/wjr.v15.i3.69 Copyright ©The Author(s) 2023.

Figure 5 Imaging features of parathyroid adenomas on four-dimensional computed tomography. CT: Computed tomography.

4D CT

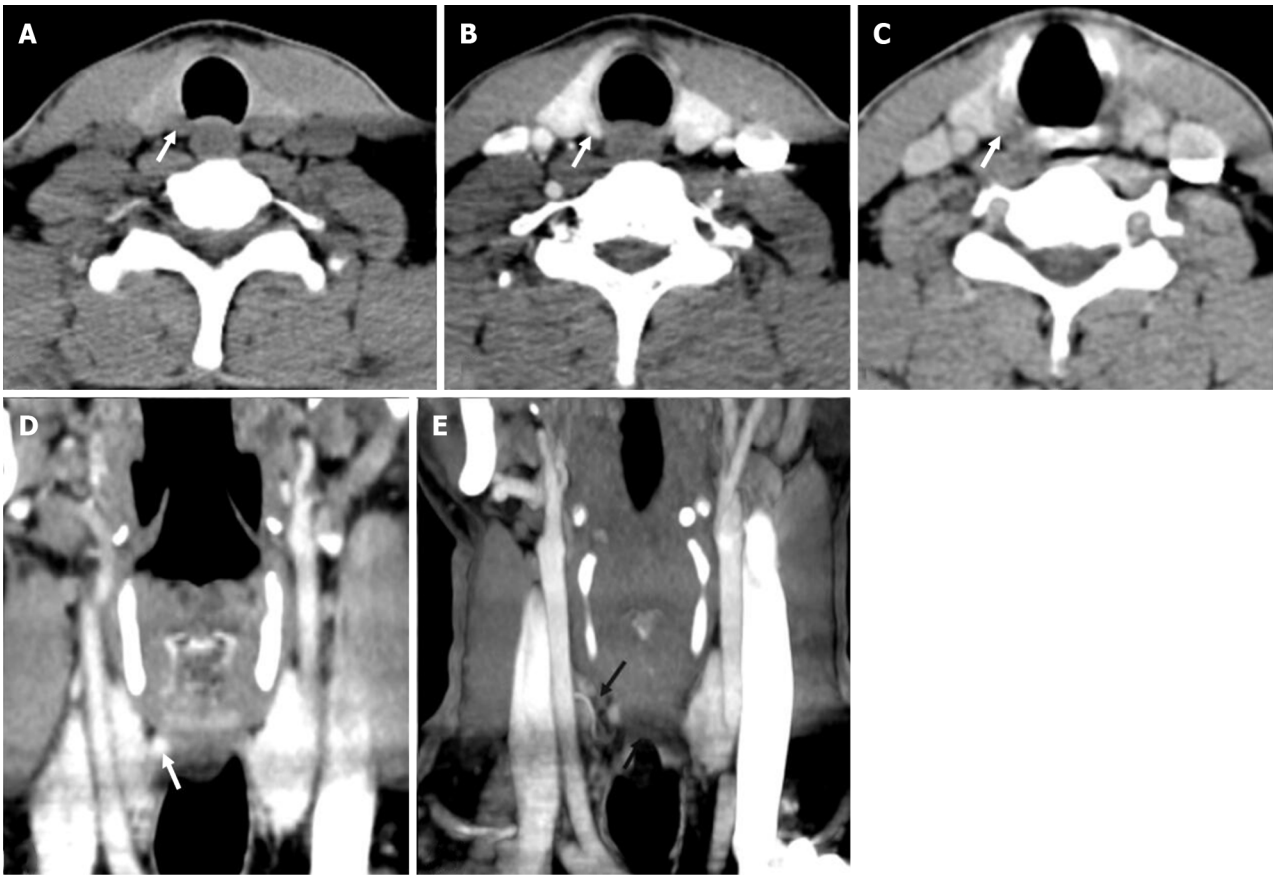
4D CT is advantageous over both ultrasonography and nuclear imaging studies in the precise localisation of both orthotopic and ectopic glands and better differentiation of parathyroid adenomas from mimics like lymph nodes and thyroid nodules (Table 1)[29]. 4D-CT demonstrates an accuracy of 93%. 4D-CT has a suboptimal 44% sensitivity, but 100% specificity, for multigland disease[30].

The first three dimensions in 4D CT are the three planes of image interpretation - axial, sagittal and coronal, while the fourth dimension refers to the change in enhancement pattern with time in the non-contrast, arterial and delayed (venous) phases (Figure 5).

Streak artifacts from hyperattenuating materials like high density contrast in neck vessels and surgical clips can hamper evaluation. The streak artifact caused by venous pooling may be prevented by using a saline chase after contrast injection[29]. The beam hardening artifact caused by clavicles and the shoulder girdle can interfere with interpretation of imaging findings which may be reduced by neck elevation achieved by putting a rolled towel under the shoulders[29]. In addition, patients are advised to avoid speaking, swallowing or coughing during image acquisition to avoid motion artifacts.

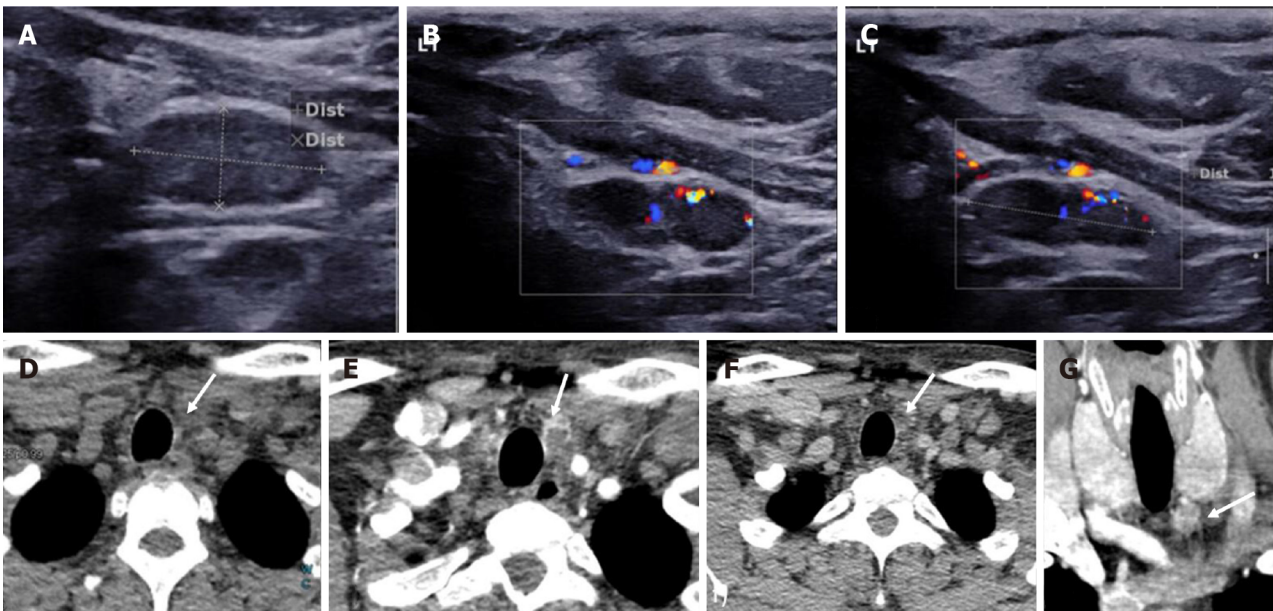
In order to facilitate the precise detection of parathyroid adenomas, Hoang *et al*[29] described a systematic five step approach: (1) Search for potential ectopic lesions in the arterial phase (2) Search for potential ectopic lesions in the arterial phase (3) Review the pattern of enhancement on other phases (4) Evaluate the morphological appearance; and (5) Correlate the computed tomography (CT) findings with other imaging modalities and clinical history. The characteristic imaging findings of a parathyroid adenoma are low attenuation on the non-contrast image, intense arterial enhancement (138-180 HU) and wash-out in the venous phase (Figures 6 and 7)[31,32]. The low attenuation on non-contrast images is important to differentiate from thyroid lesions, which are hyperdense on non-contrast CT owing to the iodine content. The typical search should start from the most common location of parathyroid adenoma *i.e.*, around the thyroid gland. This should be followed by a keen search along the expected path of migration of parathyroid glands *i.e.*, superiorly extending from the level of carotid bifurcation to the carina inferiorly. Rarer sites of ectopic parathyroid adenomas like the retropharyngeal space and intrathyroidal locations should also be screened (Figures 8-11).

Since the ultimate goal of imaging is to facilitate precise operative planning, it is important to provide the surgeon with relevant information while reporting parathyroid adenomas preferably using a predefined cartoon (Figure 1). This includes number of candidate lesions, size of the lesions, location of the lesion with respect to standard surgical landmarks (superior and inferior thyroid poles, suprasternal notch and trachea-oesophageal groove), ectopic or supernumerary parathyroid glands, underlying thyroid pathology and arterial anomalies associated with non-recurrent laryngeal nerve (aberrant right subclavian artery) which may increase risk of operative injury to the nerve[5].



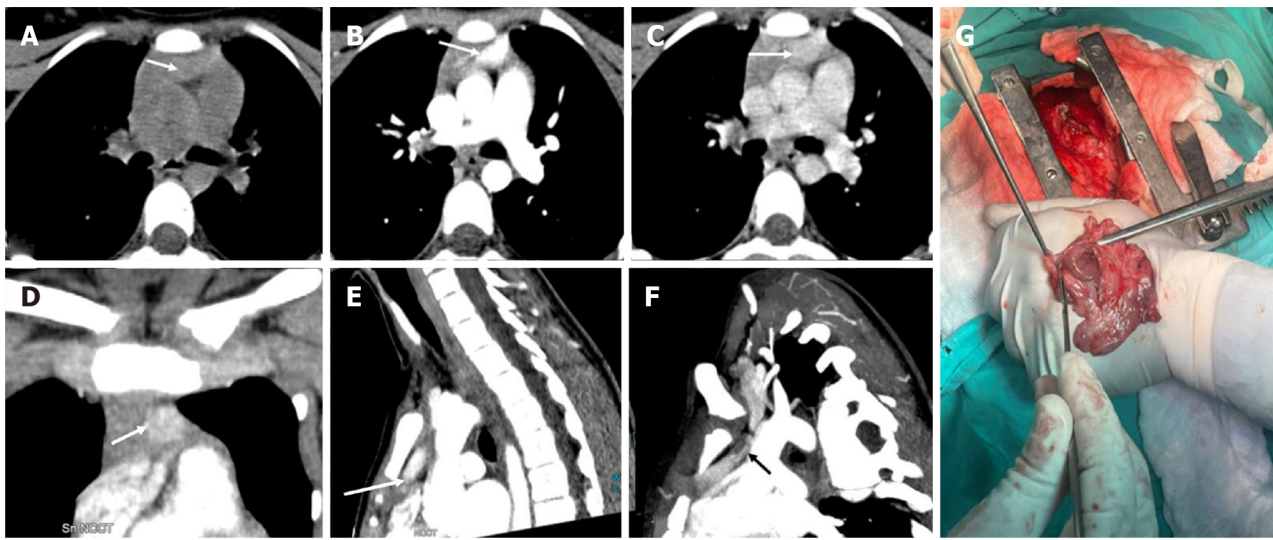
DOI: 10.4329/wjr.v15.i3.69 Copyright ©The Author(s) 2023.

Figure 6 Right superior adenoma: Four-dimensional computed tomography. A: Non-contrast computed tomography shows a small oval hypodense lesion which shows B: Intense enhancement on the arterial phase; C: Washout on the venous phase consistent with right superior parathyroid adenoma; D: Coronal image and E: Coronal maximum intensity projection image in the arterial phase better demonstrate the lesion with the feeding vessel (black arrow).



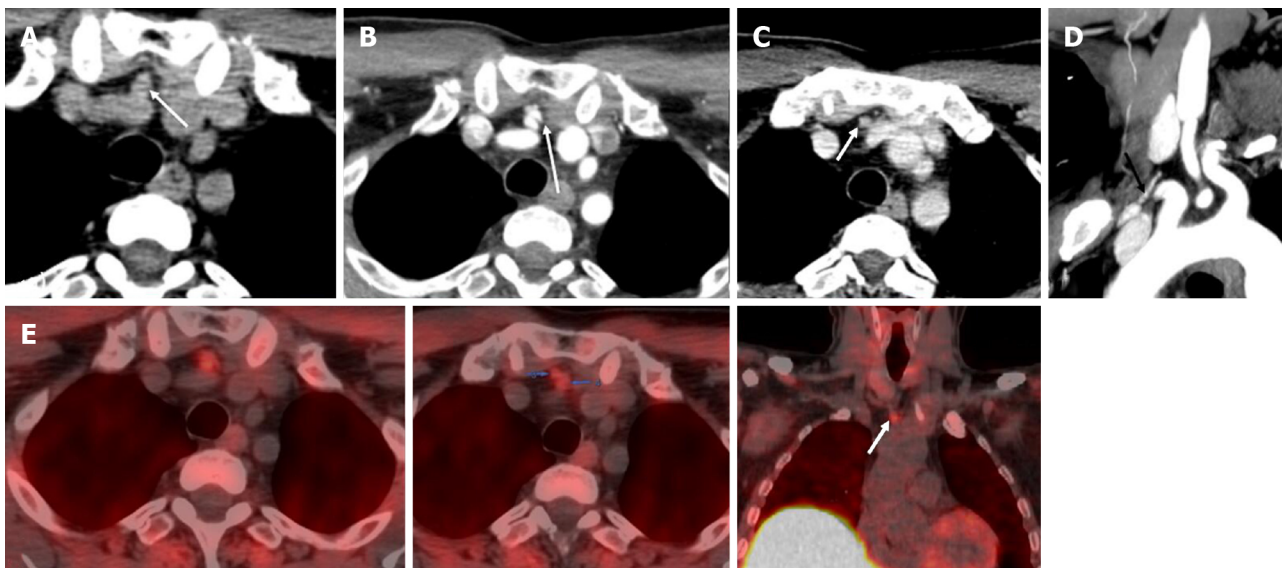
DOI: 10.4329/wjr.v15.i3.69 Copyright ©The Author(s) 2023.

Figure 7 Left inferior parathyroid adenoma. In a patient with raised parathormone levels (290 IU), grey scale ultrasound A: and colour doppler flow imaging; B and C: Showed a hypoechoic lesion with vascularity just below the left lobe of the; D: 4-dimensional computed tomography showed the lesion to be hypodense on noncontrast computer tomography; E: Hyperenhancing with central necrosis on arterial phase; F: Washout on the venous phase; G: Coronal image better demonstrates the lesion.



DOI: 10.4329/wjr.v15.i3.69 Copyright ©The Author(s) 2023.

Figure 8 Ectopic parathyroid adenoma in the anterior mediastinum. A: 4-dimensional computed tomography done in the 12-year-old female with hyperparathyroidism showed a well-defined lesion in the anterior mediastinum just behind the sternum which was hypodense on non-contrast computed tomography; B: intense arterial enhancement; C: washout on the venous phase; D: Multiplanar reformatted coronal; E: sagittal images in the arterial phase show the lesion better; F: Oblique sagittal maximum intensity projection image shows the feeding vessel (black arrow); G: Sternotomy followed by thymectomy was done and the thymus opened - the adenoma can be seen within the thymic parenchyma as pointed by the forceps.

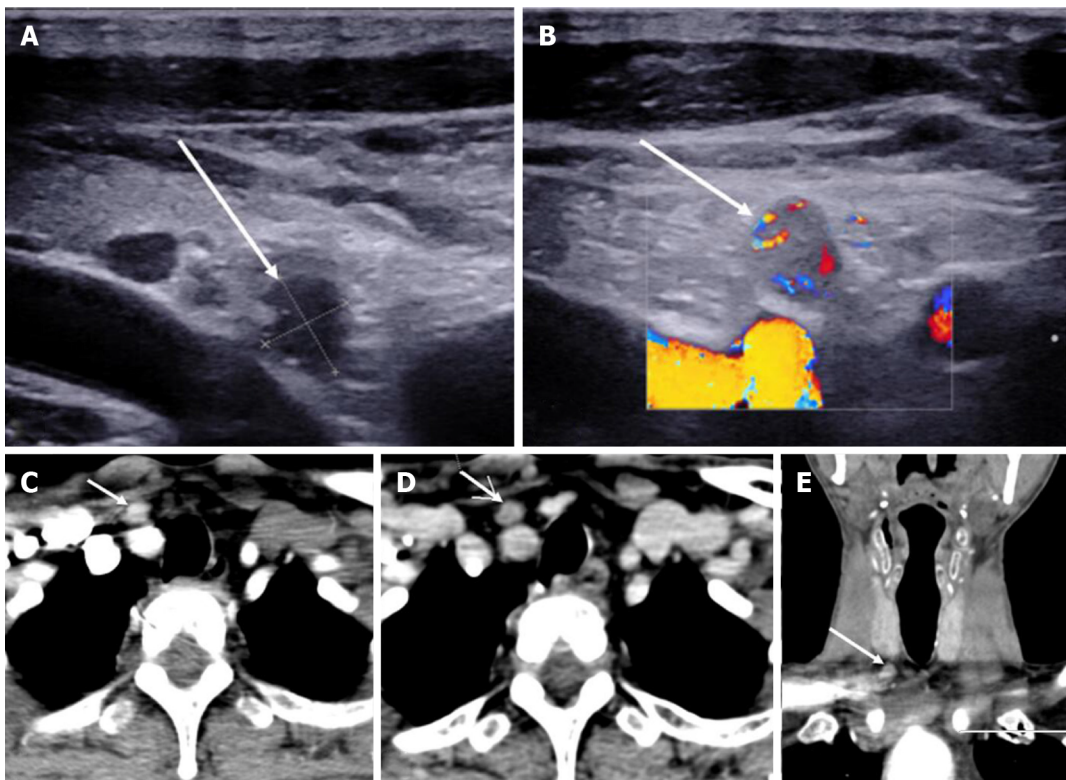


DOI: 10.4329/wjr.v15.i3.69 Copyright ©The Author(s) 2023.

Figure 9 Ectopic parathyroid adenoma in the anterior mediastinum. A: Computed tomography in a 45-year-old male patient showed a well-defined ovoid lesion in the prevascular space just posterior to the sternal notch and anterior to the inferior thyroid vessels appearing hypodense on the non-contrast phase; B: Showing intense enhancement on the arterial phase; C: washout in the venous phase; D: Coronal maximum intensity projection image demonstrates the inferior thyroid artery supplying the lesion (feeding vessel - black arrows); E: Fluoro-choline positron emission tomography shows a small tracer avid lesion in ectopic location which correlates with the computed tomography images.

Exophytic thyroid nodules and level VI cervical lymph nodes can mimic parathyroid adenomas as they have similar shape and locations. The differentiation may be done on the basis of contrast enhancement patterns. Thyroid nodules show high attenuation on the non-contrast image owing to their high iodine content and show delayed enhancement as compared to parathyroid adenoma. Lymph nodes although similar in shape to parathyroid adenomas can be differentiated from the latter based on contrast kinetics. Lymph nodes show progressive enhancement on the delayed phase as compared to parathyroid adenomas which show washout of contrast.

The detection of one lesion should not give a false sense of satisfaction to the radiologist since multiglandular disease can occur in 10% of the cases[33]. Hence, a relook is always suggested.



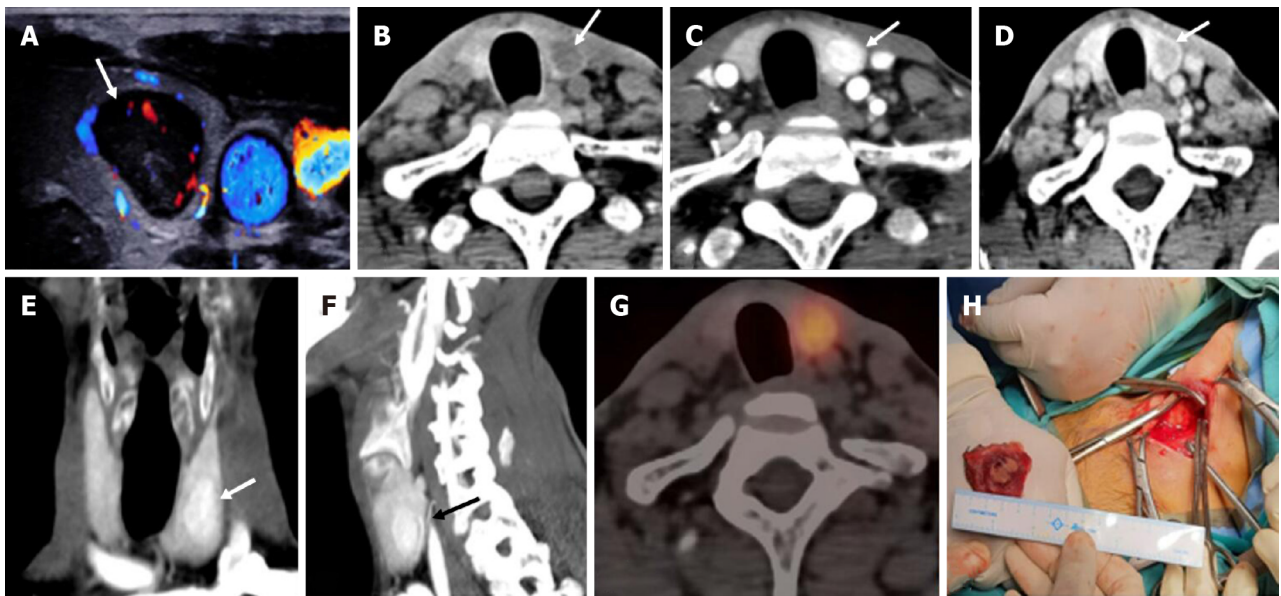
DOI: 10.4329/wjr.v15.i3.69 Copyright ©The Author(s) 2023.

Figure 10 Ectopic Parathyroid Adenoma in the Supraclavicular fossa. A: Grey scale ultrasound of the neck on a 49-year-old male patient, with history of bilateral renal stones and elevated parathormone reveals a hypoechoic lesion in the right supraclavicular location; B: On color doppler, internal vascularity was detected; C: 4-dimensional computed tomography showed a lesion with arterial enhancement; D: Washout seen on the venous phase; E: Coronal reformatted image better depicts the ectopic parathyroid adenoma in the right supraclavicular fossa.

While 4D CT is an excellent modality for detection of parathyroid adenomas, it does involve considerable radiation exposure. The effective dose is 10.4 mSv for 4D CT as compared to 7.8 mSv for nuclear scintigraphy, however 4D CT is associated with 50 times higher organ dose to the thyroid gland which becomes a cause of concern in young females since it increases the life time risk of development of thyroid cancer[34].

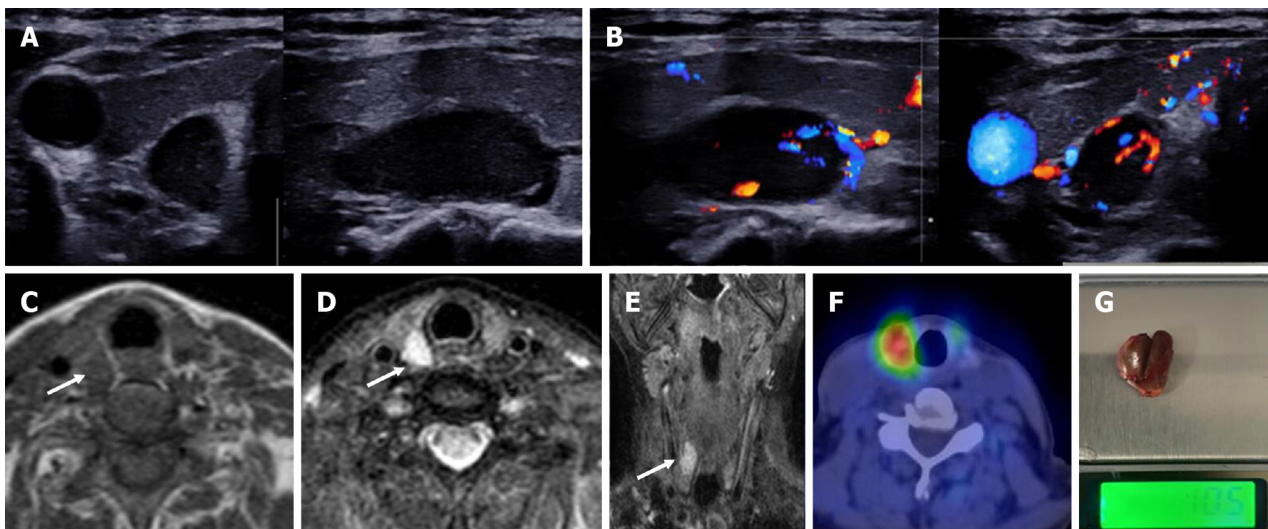
MRI

MRI is often not used as a first line modality. It is more commonly used as problem solving modality in patients with recurrent or residual disease. The non-involvement of ionizing radiation makes it a safer modality as compared to 4D CT and nuclear imaging studies; however, the modality is time consuming and isn't readily available. On a 1.5 T MRI machine, the sensitivity is 80% [35-37]. Benign parathyroid lesions are seen as well-circumscribed ovoid lesions with a cleavage plane with the thyroid tissue which is best seen on out of phase images[37]. The signal characteristics of parathyroid adenomas vary on MRI, but most commonly they tend to show homogeneously hyperintense signal on T2 weighted images (Figure 12)[37]. Post gadolinium injection, they show rapid enhancement in the arterial phase. Solid parathyroid lesions show higher signal on diffusion weighted images as compared to the other anatomically neighbouring structures in the neck thus helping in differentiation from the former[38]. 4D MRI is a novel method which has been explored in the imaging of parathyroid adenomas. The sensitivity of 4D MRI was 90% and after optimisation, 100% and the specificity was 90% [39]. 4D MRI has similar accuracy to 4D CT for the detection of parathyroid lesions. However, 4D MRI has the advantage of lack of exposure to ionizing radiation, which can be beneficial in younger patients[40]. The protocol used is the acquisition of fast T1 VIBE sequences in the axial plane prior to and after administration of gadolinium acquiring the images every 13 s for 10 sequential scans[39]. Parathyroid adenomas showed fast enhancement after 26-30 s similar to their pattern on 4D CT[39].



DOI: 10.4329/wjr.v15.i3.69 Copyright ©The Author(s) 2023.

Figure 11 Intrathyroidal parathyroid adenoma. In a patient with raised parathormone (208 IU), A: Color doppler ultrasound of the neck showed a circumscribed solid hypoechoic lesion within the left lobe of thyroid gland; B: 4-dimensional computed tomography revealed the lesion to be hypodense as compared to thyroid tissue on non-contrast; C: showed intense arterial hyperenhancement; D: Washout on the venous phase, consistent with the diagnosis of intra-thyroid parathyroid adenoma; E and F: Coronal (E) and Sagittal maximum intensity projection images better depict the lesions with vascular pedicle (black arrow) seen supplying the lesion (F); G: Single photon emission computed tomography image showing a thyroid nodule which is mildly tracer avid; H: Left hemithyroidectomy was done and the cut open section confirmed the presence of the tumor.



DOI: 10.4329/wjr.v15.i3.69 Copyright ©The Author(s) 2023.

Figure 12 Right superior parathyroid adenoma. A 50-year-old female with raised parathormone levels (96 IU) was examined using duplex ultrasound for parathyroid glands. A: Grey scale sonography in the transverse and longitudinal plane showed a well circumscribed lesion posterior to the right lobe of thyroid gland and separated from it by a clear fat plane; B: Colour doppler image shows a feeding vessel. Corroborative magnetic resonance imaging axial images show a subcentimetric lesion (arrows) posterior to the middle third of the right lobe of thyroid gland which is C: T1 hypointense; D: T2 hyperintense; E: Coronal T2w image better demonstrates the lesion; F: Correlative single photon emission computed tomography component of MIBI scan showing tracer avid lesion at the superior pole of the right lobe of thyroid; G: Image of the resected adenoma weighing 1.05 g.

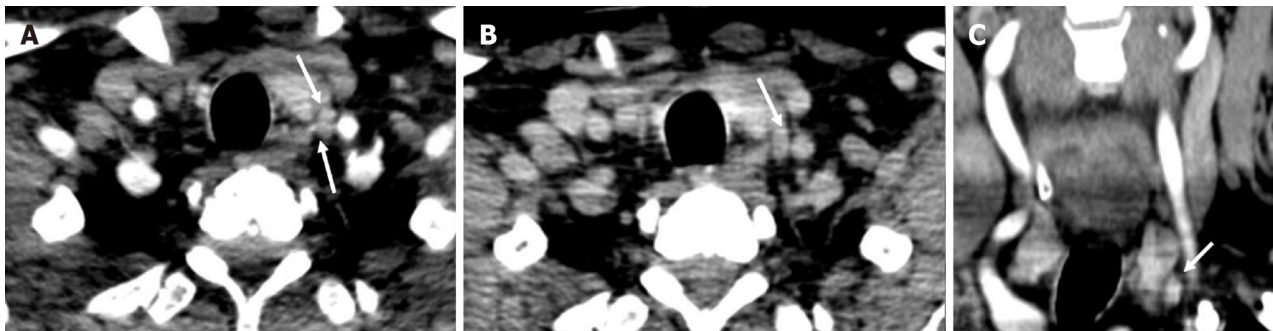
CHOLINE POSITRON EMISSION TOMOGRAPHY

Positron emission tomography (PET) is a non-invasive nuclear imaging study which provides both anatomical and functional information post intravenous injection of a radio-tracer agent. Choline labelled with positron emitters like carbon-11 or fluorine-18 is used for parathyroid imaging[41]. Increased choline uptake can be seen in parathyroid adenomas owing to the parathormone induced upregulation of choline kinase[42]. The image acquisition is done with the patient in a supine position

Table 2 Differentiating features of various parathyroid lesions

	Parathyroid hyperplasia	Parathyroid adenoma	Parathyroid carcinoma
USG	Small; Ovoid; Well-circumscribed; Homogeneously hypoechoic; Calcifications uncommon; No local invasion; CEUS - Homogeneous enhancement	Small; Ovoid; Well-circumscribed; Homogeneously hypoechoic; Calcifications uncommon; No local invasion; CEUS - Peripheral enhancement with central washout on delayed image	Large; Irregular shape; Non circumscribed margins; Heterogenous echotexture; Intra-nodular calcifications; Local invasion
CT	Small hypodense lesion (as compared to thyroid gland); Intense arterial enhancement; Washout on the venous phase; May not be identifiable on CT	Small hypodense lesion (as compared to thyroid gland); Intense arterial enhancement; Washout on the venous phase	Lesions may show infiltration into the surrounding structures
MRI	Small sized; Well defined; Homogenous; Low on T1; High on T2; Avid enhancement	Small sized; Well defined; Homogenous; Low on T1; High on T2; Avid enhancement	Large; Ill-defined; Heterogenous

USG: Ultrasound; CT: Computed tomography; MRI: Magnetic resonance imaging; CEUS: Contrast enhanced ultrasound.



DOI: 10.4329/wjr.v15.i3.69 Copyright ©The Author(s) 2023.

Figure 13 Parathyroid carcinoma. A 62-year-old male patient with recurrent hyperparathyroidism (previously operated parathyroid carcinoma), 4-dimensional computed tomography done showed few hypodense lesions with ill-defined margins near the lower pole of the left lobe of thyroid gland which showed, A: arterial enhancement however; B: No washout on the venous phase - atypical contrast kinetics for parathyroid adenoma; C: Coronal image better demonstrates the lesion. Surgical exploration and histopathological examination revealed parathyroid carcinoma recurrence.

about 45 to 60 min post intravenous injection of 18-fluoro choline[43]. Eyeballing is used to detect lesions in the eutopic or ectopic locations with parathyroid tissue being identified as maximum standardized uptake value (SUV max) four times greater than thyroid tissue[44]. Fluoro-choline PET can identify abnormal parathyroid gland in 92% patients in whom ultrasound and other nuclear imaging studies are negative[45]. It has excellent ability to detect small adenomas. The radiation dose is around 6 mSv which is lesser than that involved in MIBI scan and 4D CT. The scan involves a single acquisition as compared to the MIBI scan which involves imaging at two time points[46]. Choline is highly sensitive in the detection of parathyroid adenomas especially in multi-glandular disease. The high lesion to thyroid ratio improves the ability to detect smaller lesions. There are however several limitations with choline PET which include limited availability, high cost and the absence of a standardized protocol for imaging.

CONCLUSION

The primary goal of imaging in a clinically diagnosed case of hyperparathyroidism is precise localisation of the presence of parathyroid lesions which permits accurate surgical planning. The first line imaging modalities are ultrasound of the neck and scintigraphy. The inability to localise on these modalities or discordant findings on these modalities necessitates the use of 4D CT, MRI or F-Choline PET. Novel modalities such as contrast enhanced ultrasound and shear wave elastography of the neck should be coming up in a big way as it is free of radiation as well as safe for the kidneys. The various imaging modalities may also be used to differentiate parathyroid hyperplasia, parathyroid adenoma and parathyroid carcinoma (Table 2, Figure 13), though this may not always be possible and histopathological examination is the gold standard.

FOOTNOTES

Author contributions: Gulati S, Das JC, Spalkit S wrote the paper; Chumber S and Puri G provided the surgical expertise; Damle N provided the nuclear medicine expertise. All authors were involved in careful editing of the final manuscript.

Conflict-of-interest statement: All the authors declare that they have no conflict of interest.

Open-Access: This article is an open-access article that was selected by an in-house editor and fully peer-reviewed by external reviewers. It is distributed in accordance with the Creative Commons Attribution NonCommercial (CC BY-NC 4.0) license, which permits others to distribute, remix, adapt, build upon this work non-commercially, and license their derivative works on different terms, provided the original work is properly cited and the use is non-commercial. See: <https://creativecommons.org/licenses/by-nc/4.0/>

Country/Territory of origin: India

ORCID number: CJ Das 0000-0001-6505-5940.

S-Editor: Liu JH

L-Editor: A

P-Editor: Liu JH

REFERENCES

- 1 Fraser WD. Hyperparathyroidism. *Lancet* 2009; **374**: 145-158 [PMID: 19595349 DOI: 10.1016/S0140-6736(09)60507-9]
- 2 Bunch PM, Kelly HR. Preoperative Imaging Techniques in Primary Hyperparathyroidism: A Review. *JAMA Otolaryngol Head Neck Surg* 2018; **144**: 929-937 [PMID: 30193297 DOI: 10.1001/jamaoto.2018.1671]
- 3 Bilezikian JP, Bandeira L, Khan A, Cusano NE. Hyperparathyroidism. *Lancet* 2018; **391**: 168-178 [PMID: 28923463 DOI: 10.1016/S0140-6736(17)31430-7]
- 4 Bilezikian JP, Cusano NE, Khan AA, Liu JM, Marcocci C, Bandeira F. Primary hyperparathyroidism. *Nat Rev Dis Primers* 2016; **2**: 16033 [PMID: 27194212 DOI: 10.1038/nrdp.2016.33]
- 5 Bunch PM, Randolph GW, Brooks JA, George V, Cannon J, Kelly HR. Parathyroid 4D CT: What the Surgeon Wants to Know. *Radiographics* 2020; **40**: 1383-1394 [PMID: 32678698 DOI: 10.1148/rg.2020190190]
- 6 Phitayakorn R, McHenry CR. Incidence and location of ectopic abnormal parathyroid glands. *Am J Surg* 2006; **191**: 418-423 [PMID: 16490559 DOI: 10.1016/j.amjsurg.2005.10.049]
- 7 Kuzminski SJ, Sosa JA, Hoang JK. Update in Parathyroid Imaging. *Magn Reson Imaging Clin N Am* 2018; **26**: 151-166 [PMID: 29128002 DOI: 10.1016/j.mric.2017.08.009]
- 8 Akerström G, Malmaeus J, Bergström R. Surgical anatomy of human parathyroid glands. *Surgery* 1984; **95**: 14-21 [PMID: 6691181]
- 9 Wilhelm SM, Wang TS, Ruan DT, Lee JA, Asa SL, Duh QY, Doherty GM, Herrera MF, Pasiacka JL, Perrier ND, Silverberg SJ, Solórzano CC, Sturgeon C, Tublin ME, Udelsman R, Carty SE. The American Association of Endocrine Surgeons Guidelines for Definitive Management of Primary Hyperparathyroidism. *JAMA Surg* 2016; **151**: 959-968 [PMID: 27532368 DOI: 10.1001/jamasurg.2016.2310]
- 10 Minisola S, Cipriani C, Diacinti D, Tartaglia F, Scillitani A, Pepe J, Scott-Coombes D. Imaging of the parathyroid glands in primary hyperparathyroidism. *Eur J Endocrinol* 2016; **174**: D1-D8 [PMID: 26340967 DOI: 10.1530/EJE-15-0565]
- 11 Reeder SB, Desser TS, Weigel RJ, Jeffrey RB. Sonography in primary hyperparathyroidism: review with emphasis on scanning technique. *J Ultrasound Med* 2002; **21**: 539-52; quiz 553 [PMID: 12008817 DOI: 10.7863/jum.2002.21.5.539]
- 12 Wolf RJ, Cronan JJ, Monchik JM. Color Doppler sonography: an adjunctive technique in assessment of parathyroid adenomas. *J Ultrasound Med* 1994; **13**: 303-308 [PMID: 7932996 DOI: 10.7863/jum.1994.13.4.303]
- 13 Lane MJ, Desser TS, Weigel RJ, Jeffrey RB Jr. Use of color and power Doppler sonography to identify feeding arteries associated with parathyroid adenomas. *AJR Am J Roentgenol* 1998; **171**: 819-823 [PMID: 9725323 DOI: 10.2214/ajr.171.3.9725323]
- 14 Kamaya A, Quon A, Jeffrey RB. Sonography of the abnormal parathyroid gland. *Ultrasound Q* 2006; **22**: 253-262 [PMID: 17146333 DOI: 10.1097/01.ruq.0000237260.33509.4f]
- 15 Johnson NA, Yip L, Tublin ME. Cystic parathyroid adenoma: sonographic features and correlation with 99mTc-sestamibi SPECT findings. *AJR Am J Roentgenol* 2010; **195**: 1385-1390 [PMID: 21098199 DOI: 10.2214/AJR.10.4472]
- 16 Chandramohan A, Sathyakumar K, John RA, Manipadam MT, Abraham D, Paul TV, Thomas N, Paul MJ. Atypical ultrasound features of parathyroid tumours may bear a relationship to their clinical and biochemical presentation. *Insights Imaging* 2014; **5**: 103-111 [PMID: 24293304 DOI: 10.1007/s13244-013-0297-x]
- 17 Polga JP, Balikian JP. Partially calcified functioning parathyroid adenoma. Casedemonstrated roentgenographically. *Radiology* 1971; **99**: 55-56 [PMID: 5548688 DOI: 10.1148/99.1.55]
- 18 Randel SB, Gooding GA, Clark OH, Stein RM, Winkler B. Parathyroid variants: US evaluation. *Radiology* 1987; **165**: 191-194 [PMID: 3306784 DOI: 10.1148/radiology.165.1.3306784]
- 19 Vitetta GM, Neri P, Chiecchio A, Carriero A, Cirillo S, Mussetto AB, Codegone A. Role of ultrasonography in the management of patients with primary hyperparathyroidism: retrospective comparison with technetium-99m sestamibi scintigraphy. *J Ultrasound* 2014; **17**: 1-12 [PMID: 24616746 DOI: 10.1007/s40477-014-0067-8]

- 20 **Tsai K**, Liang TZ, Grant EG, Swanson MS, Barnett B. Optimal imaging modality for diagnosis of parathyroid adenoma: Case report and review of the literature. *J Clin Transl Endocrinol Case Rep* 2020; **17**: 100065. [DOI: [10.1016/j.jecr.2020.100065](https://doi.org/10.1016/j.jecr.2020.100065)]
- 21 **Pavlovics S**, Radzina M, Niciporuka R, Ratniece M, Mikelsons M, Tauvena E, Liepa M, Prieditis P, Ozolins A, Gardovskis J, Narbutis Z. Contrast-Enhanced Ultrasound Qualitative and Quantitative Characteristics of Parathyroid Gland Lesions. *Medicina (Kaunas)* 2021; **58** [PMID: [35056309](https://pubmed.ncbi.nlm.nih.gov/35056309/) DOI: [10.3390/medicina58010002](https://doi.org/10.3390/medicina58010002)]
- 22 **Platz Batista da Silva N**, Jung EM, Jung F, Schlitt HJ, Hornung M. VueBox® perfusion analysis of contrast-enhanced ultrasound (CEUS) examinations in patients with primary hyperparathyroidism for preoperative detection of parathyroid gland adenoma. *Clin Hemorheol Microcirc* 2018; **70**: 423-431 [PMID: [30347604](https://pubmed.ncbi.nlm.nih.gov/30347604/) DOI: [10.3233/CH-189307](https://doi.org/10.3233/CH-189307)]
- 23 **Parra Ramírez P**, Santiago Hernando A, Barquiel Alcalá B, Martín Rojas-Marcos P, Lisbona Catalán A, Álvarez Escolá C. Potential Utility of Contrast-Enhanced Ultrasound in the Preoperative Evaluation of Primary Hyperparathyroidism. *J Ultrasound Med* 2019; **38**: 2565-2571 [PMID: [30693978](https://pubmed.ncbi.nlm.nih.gov/30693978/) DOI: [10.1002/jum.14949](https://doi.org/10.1002/jum.14949)]
- 24 **Ling W**, Nie J, Zhang D, Yang Q, Jin H, Ou X, Ma X, Luo Y. Role of Contrast-Enhanced Ultrasound (CEUS) in the Diagnosis of Cervical Lymph Node Metastasis in Nasopharyngeal Carcinoma (NPC) Patients. *Front Oncol* 2020; **10**: 972 [PMID: [32766127](https://pubmed.ncbi.nlm.nih.gov/32766127/) DOI: [10.3389/fonc.2020.00972](https://doi.org/10.3389/fonc.2020.00972)]
- 25 **Chen L**, Chen L, Liu J, Wang B, Zhang H. Value of Qualitative and Quantitative Contrast-Enhanced Ultrasound Analysis in Preoperative Diagnosis of Cervical Lymph Node Metastasis From Papillary Thyroid Carcinoma. *J Ultrasound Med* 2020; **39**: 73-81 [PMID: [31222782](https://pubmed.ncbi.nlm.nih.gov/31222782/) DOI: [10.1002/jum.15074](https://doi.org/10.1002/jum.15074)]
- 26 **Cui XW**, Jenssen C, Saftoiu A, Ignee A, Dietrich CF. New ultrasound techniques for lymph node evaluation. *World J Gastroenterol* 2013; **19**: 4850-4860 [PMID: [23946589](https://pubmed.ncbi.nlm.nih.gov/23946589/) DOI: [10.3748/wjg.v19.i30.4850](https://doi.org/10.3748/wjg.v19.i30.4850)]
- 27 **Azizi G**, Piper K, Keller JM, Mayo ML, Puett D, Earp KM, Malchoff CD. Shear wave elastography and parathyroid adenoma: A new tool for diagnosing parathyroid adenomas. *Eur J Radiol* 2016; **85**: 1586-1593 [PMID: [27501893](https://pubmed.ncbi.nlm.nih.gov/27501893/) DOI: [10.1016/j.ejrad.2016.06.009](https://doi.org/10.1016/j.ejrad.2016.06.009)]
- 28 **Johnson NA**, Tublin ME, Ogilvie JB. Parathyroid imaging: technique and role in the preoperative evaluation of primary hyperparathyroidism. *AJR Am J Roentgenol* 2007; **188**: 1706-1715 [PMID: [17515397](https://pubmed.ncbi.nlm.nih.gov/17515397/) DOI: [10.2214/AJR.06.0938](https://doi.org/10.2214/AJR.06.0938)]
- 29 **Hoang JK**, Sung WK, Bahl M, Phillips CD. How to perform parathyroid 4D CT: tips and traps for technique and interpretation. *Radiology* 2014; **270**: 15-24 [PMID: [24354373](https://pubmed.ncbi.nlm.nih.gov/24354373/) DOI: [10.1148/radiol.13122661](https://doi.org/10.1148/radiol.13122661)]
- 30 **Chazen JL**, Gupta A, Dunning A, Phillips CD. Diagnostic accuracy of 4D-CT for parathyroid adenomas and hyperplasia. *AJNR Am J Neuroradiol* 2012; **33**: 429-433 [PMID: [22135127](https://pubmed.ncbi.nlm.nih.gov/22135127/) DOI: [10.3174/ajnr.A2805](https://doi.org/10.3174/ajnr.A2805)]
- 31 **Gafton AR**, Glastonbury CM, Eastwood JD, Hoang JK. Parathyroid lesions: characterization with dual-phase arterial and venous enhanced CT of the neck. *AJNR Am J Neuroradiol* 2012; **33**: 949-952 [PMID: [22241395](https://pubmed.ncbi.nlm.nih.gov/22241395/) DOI: [10.3174/ajnr.A2885](https://doi.org/10.3174/ajnr.A2885)]
- 32 **Beland MD**, Mayo-Smith WW, Grand DJ, Machan JT, Monchik JM. Dynamic MDCT for localization of occult parathyroid adenomas in 26 patients with primary hyperparathyroidism. *AJR Am J Roentgenol* 2011; **196**: 61-65 [PMID: [21178047](https://pubmed.ncbi.nlm.nih.gov/21178047/) DOI: [10.2214/AJR.10.4459](https://doi.org/10.2214/AJR.10.4459)]
- 33 **Ruda JM**, Hollenbeak CS, Stack BC Jr. A systematic review of the diagnosis and treatment of primary hyperparathyroidism from 1995 to 2003. *Otolaryngol Head Neck Surg* 2005; **132**: 359-372 [PMID: [15746845](https://pubmed.ncbi.nlm.nih.gov/15746845/) DOI: [10.1016/j.otohns.2004.10.005](https://doi.org/10.1016/j.otohns.2004.10.005)]
- 34 **Mahajan A**, Starker LF, Ghita M, Udelsman R, Brink JA, Carling T. Parathyroid four-dimensional computed tomography: evaluation of radiation dose exposure during preoperative localization of parathyroid tumors in primary hyperparathyroidism. *World J Surg* 2012; **36**: 1335-1339 [PMID: [22146947](https://pubmed.ncbi.nlm.nih.gov/22146947/) DOI: [10.1007/s00268-011-1365-3](https://doi.org/10.1007/s00268-011-1365-3)]
- 35 **Grayev AM**, Gentry LR, Hartman MJ, Chen H, Perlman SB, Reeder SB. Presurgical localization of parathyroid adenomas with magnetic resonance imaging at 3.0 T: an adjunct method to supplement traditional imaging. *Ann Surg Oncol* 2012; **19**: 981-989 [PMID: [21879264](https://pubmed.ncbi.nlm.nih.gov/21879264/) DOI: [10.1245/s10434-011-2046-z](https://doi.org/10.1245/s10434-011-2046-z)]
- 36 **Lopez Hänninen E**, Vogl TJ, Steinmüller T, Ricke J, Neuhaus P, Felix R. Preoperative contrast-enhanced MRI of the parathyroid glands in hyperparathyroidism. *Invest Radiol* 2000; **35**: 426-430 [PMID: [10901104](https://pubmed.ncbi.nlm.nih.gov/10901104/) DOI: [10.1097/00004424-200007000-00005](https://doi.org/10.1097/00004424-200007000-00005)]
- 37 **Sacconi B**, Argirò R, Diacinti D, Iannarelli A, Bezzi M, Cipriani C, Pisani D, Cipolla V, De Felice C, Minisola S, Catalano C. MR appearance of parathyroid adenomas at 3 T in patients with primary hyperparathyroidism: what radiologists need to know for pre-operative localization. *Eur Radiol* 2016; **26**: 664-673 [PMID: [26024849](https://pubmed.ncbi.nlm.nih.gov/26024849/) DOI: [10.1007/s00330-015-3854-5](https://doi.org/10.1007/s00330-015-3854-5)]
- 38 **Yildiz S**, Aralasmak A, Yetis H, Kilicarslan R, Sharifov R, Alkan A, Toprak H. MRI findings and utility of DWI in the evaluation of solid parathyroid lesions. *Radiol Med* 2019; **124**: 360-367 [PMID: [30607865](https://pubmed.ncbi.nlm.nih.gov/30607865/) DOI: [10.1007/s11547-018-0970-8](https://doi.org/10.1007/s11547-018-0970-8)]
- 39 **Merchavy S**, Luckman J, Guindy M, Segev Y, Khaffif A. 4D MRI for the Localization of Parathyroid Adenoma: A Novel Method in Evolution. *Otolaryngol Head Neck Surg* 2016; **154**: 446-448 [PMID: [26598499](https://pubmed.ncbi.nlm.nih.gov/26598499/) DOI: [10.1177/0194599815618199](https://doi.org/10.1177/0194599815618199)]
- 40 **Murugan N**, Kandasamy D, Sharma R, Goyal A, Gupta AK, Tandon N, Gupta N, Goswami R, Vurthalur S, Damle N, Agrawal S. Comparison of 4DMRI and 4DCT for the preoperative evaluation of patients with primary hyperparathyroidism. *Eur J Radiol* 2021; **138**: 109625 [PMID: [33714845](https://pubmed.ncbi.nlm.nih.gov/33714845/) DOI: [10.1016/j.ejrad.2021.109625](https://doi.org/10.1016/j.ejrad.2021.109625)]
- 41 **Vallabhajosula S**. (18)F-labeled positron emission tomographic radiopharmaceuticals in oncology: an overview of radiochemistry and mechanisms of tumor localization. *Semin Nucl Med* 2007; **37**: 400-419 [PMID: [17920348](https://pubmed.ncbi.nlm.nih.gov/17920348/) DOI: [10.1053/j.semnuclmed.2007.08.004](https://doi.org/10.1053/j.semnuclmed.2007.08.004)]
- 42 **Ishizuka T**, Kajita K, Kamikubo K, Komaki T, Miura K, Nagao S, Nozawa Y. Phospholipid/Ca²⁺-dependent protein kinase activity in human parathyroid adenoma. *Endocrinol Jpn* 1987; **34**: 965-968 [PMID: [3450512](https://pubmed.ncbi.nlm.nih.gov/3450512/) DOI: [10.1507/endoerj1954.34.965](https://doi.org/10.1507/endoerj1954.34.965)]
- 43 **Tay D**, Das JP, Yeh R. Preoperative Localization for Primary Hyperparathyroidism: A Clinical Review. *Biomedicines* 2021; **9** [PMID: [33917470](https://pubmed.ncbi.nlm.nih.gov/33917470/) DOI: [10.3390/biomedicines9040390](https://doi.org/10.3390/biomedicines9040390)]
- 44 **Parvinian A**, Martin-Macintosh EL, Goenka AH, Durski JM, Mullan BP, Kemp BJ, Johnson GB. (11)C-Choline PET/CT for Detection and Localization of Parathyroid Adenomas. *AJR Am J Roentgenol* 2018; **210**: 418-422 [PMID: [29140118](https://pubmed.ncbi.nlm.nih.gov/29140118/) DOI: [10.2214/AJR.17.18312](https://doi.org/10.2214/AJR.17.18312)]

- 45 **Michaud L**, Burgess A, Huchet V, Lefèvre M, Tassart M, Ohnona J, Kerrou K, Balogova S, Talbot JN, Périé S. Is 18F-fluorocholine-positron emission tomography/computerized tomography a new imaging tool for detecting hyperfunctioning parathyroid glands in primary or secondary hyperparathyroidism? *J Clin Endocrinol Metab* 2014; **99**: 4531-4536 [PMID: 25215560 DOI: 10.1210/jc.2014-2821]
- 46 **Kluijfhout WP**, Vorselaars WM, Vriens MR, Borel Rinkes IH, Valk GD, de Keizer B. Enabling minimal invasive parathyroidectomy for patients with primary hyperparathyroidism using Tc-99m-sestamibi SPECT-CT, ultrasound and first results of (18)F-fluorocholine PET-CT. *Eur J Radiol* 2015; **84**: 1745-1751 [PMID: 26047823 DOI: 10.1016/j.ejrad.2015.05.024]

Magnetic resonance imaging findings of spontaneous pyomyoma in a premenopausal woman managed with myomectomy: A case report

David Martínez, Gustavo E Sanchez, Jhonatan Gómez, Luis J Sonda, Luis D Suárez, Carlos S López, Juan J Vega, Daniel A Cepeda

Specialty type: Radiology, nuclear medicine and medical imaging

Provenance and peer review: Unsolicited article; Externally peer reviewed.

Peer-review model: Single blind

Peer-review report's scientific quality classification

Grade A (Excellent): 0

Grade B (Very good): 0

Grade C (Good): C, C

Grade D (Fair): 0

Grade E (Poor): E

P-Reviewer: Aydin S, Turkey; Cheng YS, China; Hegazy AA, Egypt

Received: September 1, 2022

Peer-review started: September 1, 2022

First decision: November 25, 2022

Revised: January 24, 2023

Accepted: March 9, 2023

Article in press: March 9, 2023

Published online: March 28, 2023



David Martínez, Gustavo E Sanchez, Department of Radiology, Hospital Christus Muguerza, Puebla 72501, Puebla, Mexico

Jhonatan Gómez, Department of Radiology, Hospital Regional Dr. Juan Graham Casasús, Villahermosa 86126, Tabasco, Mexico

Luis J Sonda, Luis D Suárez, Carlos S López, Juan J Vega, Daniel A Cepeda, Department of Radiology, Hospital de Especialidades 5 de Mayo, Puebla 72550, Puebla, Mexico

Corresponding author: David Martinez, MD, Doctor, Department of Radiology, Hospital Christus Muguerza, Av. 11 Ote. 1826, Azcarate, 72501 Puebla, Puebla, Mexico.
www_david_atmsn.com

Abstract

BACKGROUND

Acute fibroid complications are rare. However, failure to recognize and treat acute complications expeditiously when they occur can lead to catastrophic, even deadly, complications. Pyomyoma is a rare but potentially fatal condition resulting from infarction and infection of a fibroid through bacterial seeding and direct, hematogenous, or lymphatic dissemination. Even though the diagnosis is established through clinical and laboratory findings, imaging is an important complementary method to support the suspected diagnosis.

CASE SUMMARY

Herein, we report a case of a pyomyoma in a nulliparous woman previously diagnosed with uterine leiomyomatosis according to ultrasound findings. The patient had previously attended the emergency room due to hypogastric pain unresponsive to analgesics. After a week of persistent pain, she developed sepsis without any identifiable foci. Magnetic resonance imaging revealed findings compatible with uterine myomatosis with red degeneration, and a possible diagnosis of a pyomyoma was made according to the imaging findings along with the patient's clinical features. We decided to perform myomectomy (which is an infrequently performed surgical treatment due to the procedure's intrinsic implications) due to the patient's desire to preserve fertility. Histopathologic results revealed a uterine leiomyoma with coagulative and liquefactive necrosis, while the tissue culture showed gram-negative cocci bacteria, which were successfully treated using antibiotic therapy. The patient's health status improved after several

days.

CONCLUSION

The main diagnostic tools to evaluate pyomyomas are the clinical and laboratory findings as well as tissue cultures. Nonetheless, magnetic resonance imaging can help to corroborate these findings as well as to better characterize myomas with its different complications.

Key Words: Diffusion-weighted images; Apparent diffusion coefficient; Leiomyoma; Sepsis; Magnetic resonance imaging; Case report

©The Author(s) 2023. Published by Baishideng Publishing Group Inc. All rights reserved.

Core Tip: Pyomyoma is a rare but potentially fatal condition resulting from infarction and infection of a fibroid through bacterial seeding and direct, hematogenous, or lymphatic dissemination. Diffusion-weighted images, apparent diffusion coefficient quantification and the addition of T1- and T2-weighted sequences with fat suppression can improve the characterization of the components of a myoma during degeneration.

Citation: Martínez D, Sanchez GE, Gómez J, Sonda LJ, Suárez LD, López CS, Vega JJ, Cepeda DA. Magnetic resonance imaging findings of spontaneous pyomyoma in a premenopausal woman managed with myomectomy: A case report. *World J Radiol* 2023; 15(3): 83-88

URL: <https://www.wjgnet.com/1949-8470/full/v15/i3/83.htm>

DOI: <https://dx.doi.org/10.4329/wjr.v15.i3.83>

INTRODUCTION

A pyomyoma is a rare but potentially fatal condition resulting from infarction and infection of a leiomyoma[1] through bacterial seeding and direct, hematogenous, or lymphatic dissemination. Because of the rarity of pyomyomas, low clinical suspicion delays its diagnosis and predisposes patients to possible complications, such as purulent peritonitis or sepsis.

The definitive treatment of a pyomyoma is hysterectomy[2]. An alternative consists of intravenous administration of broad-spectrum antibiotics and myomectomy. Surgery can be adjusted according to the size and number of pyomyomas while considering the future reproductive wishes of the patient[3]. Surgery can also be performed to make a definitive diagnosis[1] while decreasing associated morbidity and mortality[4].

While ultrasound and computed tomography are often the first tools used for the detection of pyomyomas[5], magnetic resonance imaging (MRI) is the most precise imaging technique that can be used to characterize myomas with different types of degeneration (including the identification of purulent collections in the pyomyoma), which makes it potentially useful for diagnosis. However, the emergency use of MRI is still controversial[5].

Differential diagnoses of pyomyoma include gynecological tumors (benign or malignant ovarian tumors, tubo-ovarian abscess, uterine sarcoma, or pyometra), endometritis, gastrointestinal stromal tumors, and appendiceal mucocele[3,5]. However, red degeneration should be considered as an important entity due to its similarities to a pyomyoma on MRI. Red degeneration can exhibit peripheral or diffused hyperintensities in T1-weighted images and variable signal intensity, with or without a hypointense rim in T2-weighted images[5]. As an additional complementary sequence, diffusion-weighted imaging can be obtained. Generally, tissues with high cellularity have lower diffusion coefficients, which can be clinically related to purulent materials.

The ethics committee of hospital Christus Muguerza Hospital Betania approved this study. A signed informed consent by the patient was obtained for the publication of this case report.

CASE PRESENTATION

Chief complaints

A 26-year-old premenopausal nulliparous woman was evaluated for severe hypogastric pain in the prior 24 h with no response to analgesics.

History of present illness

The patient had a history of uterine myomatosis, which was confirmed by a pelvic ultrasound. She was prescribed with analgesics and sent home; however, she returned to the emergency department of our hospital a week later with abnormal uterine bleeding and abdominal pain.

History of past illness

The patient had no prior chronic or systemic disease. The patient had no prior surgeries.

Personal and family history

The patient did not have prior pregnancies or deliveries. Her menstrual cycle was reported as regular. There was no family history of chronic diseases or cancer.

Physical examination

A depressible and tender abdomen with a slight increase in volume in the hypogastrium was observed during the physical examination.

Laboratory examinations

On admission, there were no abnormal laboratory findings. A reverse transcription PCR for severe acute respiratory syndrome coronavirus 2 was obtained, with a negative result.

Imaging examinations

Requested MRI showed a mass located in the posterior wall of the uterus, with a T1- and T2-weighted hyperintense component, a T1-weighted hyperintense halo as well as some materials with high T1-weighted fat-saturation signal (suggesting a hematic content) and content with high T2-weighted fat-saturation signal indicating liquid content (Figure 1). In the diffusion-weighted images, an apparent diffusion coefficient map was obtained by measuring the region of interest with a low apparent diffusion coefficient (ADC) value ($1.5 \times 10^{-3} \text{ mm}^2/\text{s}$) (Figure 2). The results obtained suggested the presence of a leiomyoma with red degeneration; however, pyomyoma was considered as a differential diagnosis due to the low ADC value.

FINAL DIAGNOSIS

The final given diagnosis was uterine myomatosis with red degeneration complicated with pyomyoma.

TREATMENT

After evaluating the case and considering that the patient was a nulliparous woman, a laparoscopic myomectomy was performed to preserve the patient's fertility wishes (Figure 3). This also resulted in the discovery of an intraoperative large myoma that was peripherally hypovascularized with friable tissue in its center.

OUTCOME AND FOLLOW-UP

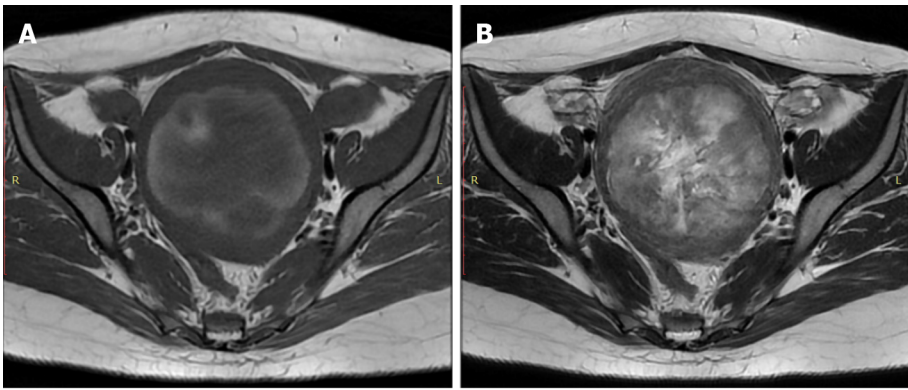
At 12 h postoperatively, the patient experienced sepsis symptoms, consisting of hypotension (70/40 mmHg), tachycardia (150 bpm), fever (39.8 °C), respiratory distress (30 rpm; SPO₂ 80%), and drowsiness. Therefore, she was admitted to the intensive care unit for management with oxygen therapy, fluid resuscitation, and empiric antibiotic therapy.

After performing myomectomy, laboratory results were obtained, showing anemia (10.4 g/dL), leukocytosis with bandemia (18.32 K/uL; 10.0%), high C-reactive protein levels (123.94 mg/L), procalcitonin (5.55 ng/mL), pCO₂ (31.0 mmHg), HCO₃ (20.6), BEb (-2.5), and lactate (1.3).

The histopathologic report showed a uterine leiomyoma with coagulative and liquefactive necrosis, while a tissue culture showed gram-negative cocci bacteria, which confirmed the diagnosis of a pyomyoma. Antibiotic treatment was adjusted towards gram-negative cocci, resulting in normalization of inflammatory markers and clinical improvement after 3 d.

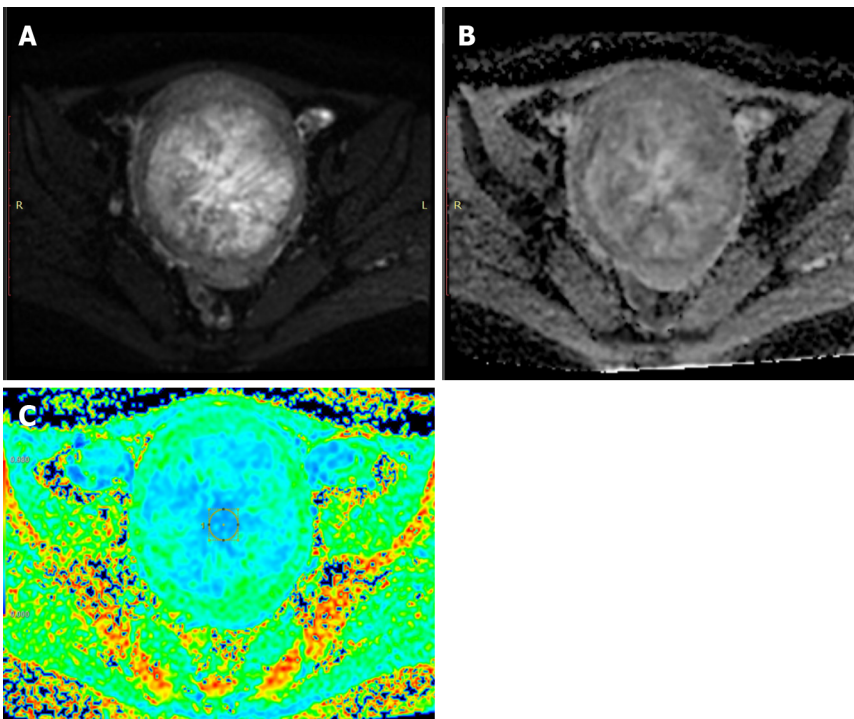
DISCUSSION

Myomas are the most common solid pelvic tumor in women during reproductive years, occurring in



DOI: 10.4329/wjr.v15.i3.83 Copyright ©The Author(s) 2023.

Figure 1 Magnetic resonance imaging findings. An axial view T1 and T2-weighted showed a large intramural lesion in the myometrium with materials. A: High-signal intensity in T1-weighted view indicated the presence of a hemorrhagic component; B: High-signal intensity material in T2-weighted view indicated the presence of a liquid component.



DOI: 10.4329/wjr.v15.i3.83 Copyright ©The Author(s) 2023.

Figure 2 Magnetic resonance imaging findings by diffusion-weighted images. A: An axial diffusion-weighted view showed areas with restrictions; B: Apparent diffusion coefficient map; C: Apparent diffusion coefficient color map.

approximately 20%-40% of this population[6]. It is estimated that 50% of women bearing myomas will remain asymptomatic through their lives. Also known as fibroids or leiomyomas, these tumors are benign and originate from smooth muscle cells of the uterus, but cases have been reported in which smooth muscle from uterine blood vessels may become their source[6]. The remaining 50% of women will develop symptoms related to their size, location, or degenerative changes, if present. Some of these symptoms may include polymenorrhea, hypermenorrhea, or even menometrorrhagia[6].

Associated pain in myomatosis is relatively infrequent, and it usually presents upon certain criteria: (1) Fibroids above 5 cm; (2) Posterior wall fibroids; and (3) Fibroids with a sudden increase in size (often related to pregnancy) as the blood supply may become insufficient, producing tissue anoxia, necrotic infarction, and the subsequent release of prostaglandins[7]. Cases of severe pain are often associated with torsion of pedunculated myomas, cervical dilation by submucosal myomas, and fibroid red degeneration of the pregnancy[7]. All of these conditions usually call for immediate action.

In this reviewed case, the patient had a previous history of myomatosis and presented with acute persistent pain, which prompted an ultrasound evaluation. The study did not show relevant changes within myomas. On ultrasound, a painful myoma above 200 cm³ with changes in the echogenicity



DOI: 10.4329/wjr.v15.i3.83 Copyright ©The Author(s) 2023.

Figure 3 Follow-up magnetic resonance imaging. A: Sagittal T2-weighted image showed an intramural lesion before surgery; B: Sagittal T2-weighted image showed an intramural lesion after myomectomy.

suggesting internal cystic lesions can suggest red degeneration and infarction[7]. Even so, according to clinical suspicion, an MRI was ordered to exclude complications from the myomas, considering that red degeneration is an important complication of leiomyomas.

Myomas with red degeneration are characterized by acute onset abdominal pain, mild fever, localized tenderness over the myoma (as in this case), and leukocytosis. As mentioned before, they can become infected and turn to pyomyomas. Extensive necrotic areas can become infected with anaerobic bacteria. MRI should be considered in such situations to confirm the diagnosis and facilitate fibroid mapping before surgery. Pyomyomas usually lead to inflammatory changes and tissue necrosis, compatible with those present at the moment of presentation in this case, arising suspicion due to the low ADC on MRI[7].

Patients with a history of myomatosis who develop sepsis with unidentifiable foci should be suspected for pyomyoma. In our case, sepsis occurred after the surgical procedure. However, according to available literature, the clinical picture can be very unspecific, and the clinical presentation of pyomyomas can be insidious. Therefore, the diagnosis could be complicated.

CONCLUSION

The main diagnostic tools to evaluate pyomyomas are the clinical and laboratory findings as well as tissue cultures. Nonetheless, MRI can help to corroborate these findings as well as to better characterize myomas along with its complications.

FOOTNOTES

Author contributions: Martínez D designed the study and wrote the manuscript; Sánchez GE wrote the manuscript; Gómez J reviewed the manuscript; Sonda LJ wrote the introduction; Suárez LD wrote the manuscript; López CS wrote the discussion; Vega JJ wrote the abstract; Cepeda DA reviewed the manuscript.

Informed consent statement: The patient provided informed written consent about personal and medical data collection prior to study enrollment.

Conflict-of-interest statement: The authors report no relevant conflicts of interest for this article.

CARE Checklist (2016) statement: The authors have read the CARE Checklist (2016), and the manuscript was prepared and revised according to the CARE Checklist (2016).

Open-Access: This article is an open-access article that was selected by an in-house editor and fully peer-reviewed by

external reviewers. It is distributed in accordance with the Creative Commons Attribution NonCommercial (CC BY-NC 4.0) license, which permits others to distribute, remix, adapt, build upon this work non-commercially, and license their derivative works on different terms, provided the original work is properly cited and the use is non-commercial. See: <https://creativecommons.org/licenses/by-nc/4.0/>

Country/Territory of origin: Mexico

ORCID number: David Martinez [0000-0003-1417-4784](https://orcid.org/0000-0003-1417-4784); Gustavo E Sanchez [0000-0003-3579-8027](https://orcid.org/0000-0003-3579-8027); Jhonatan Gomez [0000-0002-8710-8684](https://orcid.org/0000-0002-8710-8684); Luis J Sonda [0000-0002-9638-9094](https://orcid.org/0000-0002-9638-9094); Luis D Suarez [0000-0003-3463-5111](https://orcid.org/0000-0003-3463-5111); Carlos S Lopez [0000-0002-0590-7766](https://orcid.org/0000-0002-0590-7766); Juan J Vega [0000-0003-3877-3431](https://orcid.org/0000-0003-3877-3431).

S-Editor: Liu GL

L-Editor: Filipodia

P-Editor: Liu GL

REFERENCES

- 1 **Iwahashi N**, Mabuchi Y, Shiro M, Yagi S, Minami S, Ino K. Large uterine pyomyoma in a perimenopausal female: A case report and review of 50 reported cases in the literature. *Mol Clin Oncol* 2016; **5**: 527-531 [PMID: [27882238](https://pubmed.ncbi.nlm.nih.gov/27882238/) DOI: [10.3892/mco.2016.1005](https://doi.org/10.3892/mco.2016.1005)]
- 2 **Kitamura Y**, Ascher SM, Cooper C, Allison SJ, Jha RC, Flick PA, Spies JB. Imaging manifestations of complications associated with uterine artery embolization. *Radiographics* 2005; **25** Suppl 1: S119-S132 [PMID: [16227486](https://pubmed.ncbi.nlm.nih.gov/16227486/) DOI: [10.1148/rg.25si055518](https://doi.org/10.1148/rg.25si055518)]
- 3 **Karcaaltincaba M**, Sudakoff GS. CT of a ruptured pyomyoma. *AJR Am J Roentgenol* 2003; **181**: 1375-1377 [PMID: [14573437](https://pubmed.ncbi.nlm.nih.gov/14573437/) DOI: [10.2214/ajr.181.5.1811375](https://doi.org/10.2214/ajr.181.5.1811375)]
- 4 **Ono H**, Kanematsu M, Kato H, Toyoki H, Hayasaki Y, Furui T, Morishige K, Hatano Y. MR imaging findings of uterine pyomyoma: radiologic-pathologic correlation. *Abdom Imaging* 2014; **39**: 797-801 [PMID: [24615512](https://pubmed.ncbi.nlm.nih.gov/24615512/) DOI: [10.1007/s00261-014-0112-2](https://doi.org/10.1007/s00261-014-0112-2)]
- 5 **Peris H**, Del Riego J, Criado E, García-Chamón RB, Vall E, Mayoral M, Martín A. Value of diffusion-weighted magnetic resonance imaging in the diagnosis of pyomyoma. *Radiol Case Rep* 2022; **17**: 137-141 [PMID: [34820037](https://pubmed.ncbi.nlm.nih.gov/34820037/) DOI: [10.1016/j.radr.2021.10.018](https://doi.org/10.1016/j.radr.2021.10.018)]
- 6 **Wallach EE**, Vlahos NF. Uterine myomas: an overview of development, clinical features, and management. *Obstet Gynecol* 2004; **104**: 393-406 [PMID: [15292018](https://pubmed.ncbi.nlm.nih.gov/15292018/) DOI: [10.1097/01.aog.0000136079.62513.39](https://doi.org/10.1097/01.aog.0000136079.62513.39)]
- 7 **Milazzo GN**, Catalano A, Badia V, Mallozzi M, Caserta D. Myoma and myomectomy: Poor evidence concern in pregnancy. *J Obstet Gynaecol Res* 2017; **43**: 1789-1804 [PMID: [28892210](https://pubmed.ncbi.nlm.nih.gov/28892210/) DOI: [10.1111/jog.13437](https://doi.org/10.1111/jog.13437)]



Published by **Baishideng Publishing Group Inc**
7041 Koll Center Parkway, Suite 160, Pleasanton, CA 94566, USA

Telephone: +1-925-3991568

E-mail: bpgoffice@wjgnet.com

Help Desk: <https://www.f6publishing.com/helpdesk>

<https://www.wjgnet.com>

